

# *The properties and genesis environments of South Atlantic cyclones*

Article

Accepted Version

Gramscianinov, C. B., Hodges, K. I. ORCID:  
<https://orcid.org/0000-0003-0894-229X> and Camargo, R.  
(2019) The properties and genesis environments of South  
Atlantic cyclones. *Climate Dynamics*, 53 (7-8). pp. 4115-4140.  
ISSN 1432-0894 doi: 10.1007/s00382-019-04778-1 Available  
at <https://centaur.reading.ac.uk/80949/>

It is advisable to refer to the publisher's version if you intend to cite from the work. See [Guidance on citing](#).

To link to this article DOI: <http://dx.doi.org/10.1007/s00382-019-04778-1>

Publisher: Springer

All outputs in CentAUR are protected by Intellectual Property Rights law, including copyright law. Copyright and IPR is retained by the creators or other copyright holders. Terms and conditions for use of this material are defined in the [End User Agreement](#).

[www.reading.ac.uk/centaur](http://www.reading.ac.uk/centaur)

**CentAUR**

Central Archive at the University of Reading

Reading's research outputs online

1 **The Properties and Genesis Environments of South**  
2 **Atlantic Cyclones**

3 **C. B. Gramscianinov · K. I. Hodges · R.**  
4 **Camargo**

5  
6 Received: date / Accepted: date

7 **Abstract** A new climatology of South Atlantic cyclones is produced to provide  
8 new insights into the conditions leading to genesis in different regions of  
9 the domain. Cyclones are identified and tracked based on the relative vorticity  
10 at 850 hPa computed from the NCEP-CFSR winds. The characteristics  
11 of the cyclones are obtained by diagnostic variables sampled within a radial  
12 distance from the cyclone centers to produce the spatial distribution of cyclone  
13 properties at the time of genesis. Also, cyclone centered composites are  
14 used to analyze the cyclone structure and evolution during their genesis. There  
15 are four main cyclogenesis regions in the South Atlantic Ocean: the Southern  
16 Brazilian coast (SE-BR, 30°S), over the continent near the La Plata river discharge  
17 region (LA PLATA, 35°S), the southeastern coast of Argentina (ARG, 40°S-55°S)  
18 and the Southeastern Atlantic (SE-SAO, centered at 45°S and 10°W). We found  
19 that cyclogenesis northward of 35°S occurs mainly due to low-level forcing  
20 associated with moisture transport in the summer, and is associated with upper-level  
21 forcing in the winter due to a strong baroclinic environment. Southward of 35°S,  
22 cyclones develop in a high baroclinic environment throughout the year with only  
23 a small influence from moist processes. The cyclone composites reveal that SE-BR  
24 and SE-SAO cyclones are associated with secondary development, the LA PLATA  
25 cyclones development is influenced by an orographic low in their early stages,  
26 and ARG cyclones are

---

C. B. Gramscianinov  
Departamento de Ciências Atmosféricas, Instituto de Astronomia, Geofísica e Ciências Atmosféricas, Universidade de São Paulo, Rua do Matão, 1226, Cidade Universitária, São Paulo/SP - Brazil.  
E-mail: carolina.gramscianinov@alumni.usp.br

K. I. Hodges  
Department of Meteorology, University of Reading

R. Camargo  
Departamento de Ciências Atmosféricas, Instituto de Astronomia, Geofísica e Ciências Atmosféricas, Universidade de São Paulo

influenced by thermal advection as an essential mechanism in the reduction of static stability.

**Keywords** Cyclogenesis · Extratropical Cyclones · South America · Storm track

## 1 Introduction

Cyclones play a crucial role in the weather and climate of the South American continent, where the major part of the population lives in coastal cities, surrounded by regions of cyclogenesis (Gan and Rao, 1991; Sinclair, 1995; Hoskins and Hodges, 2005; Reboita et al, 2010a). Surface cyclones are responsible for the major precipitation in the Southeast of South America and the maintenance of the South Atlantic Convergence Zone (SACZ) during the South America Monsoon (Reboita et al, 2010b). Besides this, cyclones are related to several natural hazards along the coast through storm surges and flooding (e.g., Seluchi and Saulo, 1998; Parise et al, 2009), and wave generation (e.g., Innocentini and Neto, 1996; da Rocha et al, 2004) causing damage to economic activities such as oil exploration, harbors and navigation. Therefore, understanding the dynamical characteristics of these systems and their development is essential for mitigation policies and improvements in prediction methods.

During previous decades, several studies have led to a better understanding of the distribution of cyclones and their development in the Southern Hemisphere through synoptic analysis (Taljaard, 1967) and automated tracking methods, using satellite data (Streten and Troup, 1973; Satyamurty et al, 1990), operational analyses (Jones and Simmonds, 1993; Sinclair, 1994) and reanalyses (Simmonds and Keay, 2000; Hoskins and Hodges, 2005). Extratropical cyclones in the Southern Hemisphere primarily occur within  $55^{\circ}\text{S}$  to  $35^{\circ}\text{S}$  (maximum at  $45^{\circ}\text{S}$ ) and near Antarctica (e.g. Hoskins and Hodges, 2005). During the austral summer (DJF) the main storm track shifts poleward (Taljaard, 1967). The preferential orientation is in a south-southeast direction with a spiral pattern towards Antarctica in the winter (e.g., Hoskins and Hodges, 2005). In previous studies, the eastern coast of South America has always been highlighted as an important genesis region for the Southern Hemisphere.

One of the first studies with a regional focus on the South Atlantic was performed by Gan and Rao (1991) who used sea level pressure synoptic charts from 1979 to 1988 to develop a climatology of cyclogenesis in the South American region. Their study found two main genesis regions on the eastern coast of South America: one in southeast Argentina and another above Uruguay. By using vorticity instead of the pressure field, more recent works found a third genesis region on the southeastern Brazilian coast (Sinclair, 1995; Hoskins and Hodges, 2005; Reboita et al, 2010a).

The southeastern coast of Argentina, around  $45^{\circ}\text{S}$ , is the most active cyclogenesis region (Hoskins and Hodges, 2005). High values of genesis are found year round, but in the summer the occurrence of cyclogenesis is largest. For the Uruguay genesis ( $30^{\circ}\text{S}$ ) the most active period is during winter. Gan and

Rao (1991) also found the same cyclone genesis for the Argentina and Uruguay regions. The third cyclogenesis region is most active during the austral summer on the southeastern Brazilian coast (Hoskins and Hodges, 2005; Reboita et al, 2010a). Hoskins and Hodges (2005) described the last two regions as subtropical paths of the South Atlantic storm track owing to their occurrence at lower latitudes than the main storm track of the Southern Hemisphere.

The development of cyclones along the South American coast is related mainly to the high and mid-level transient troughs from the Pacific and their interaction with the stationary Andes trough (Gan and Rao, 1994; Vera et al, 2002). Mendes et al (2007) showed that the Andes Cordillera not only fosters cyclonic anomalies through lee effects but is also conducive to channeling tropical moist and warm air to subtropical latitudes generating moisture convergence at the surface. Mid-level ascent may enhance this low-level convergence promoting latent heat release due to precipitation (Vera et al, 2002).

Ocean conditions can also influence cyclogenesis along the South American coast. Vera et al (2002) suggest that the warm waters of the Brazil Current provide moisture and heat that reduces the static stability at low levels. Besides this, the presence of the Brazil-Malvinas Confluence near  $38^{\circ}\text{S}$  (Gordon, 1989) is responsible for introducing high Sea Surface Temperature (SST) gradients that can generate low-level baroclinicity (Sanders and Gyakum, 1980) promoting cyclogenesis or intensification of cyclones.

Global and hemispheric scale studies have shown cyclone spatial distributions but generally, do not allow a detailed focus on the regional features of cyclones and the storm tracks. Some studies concerning cyclones and their evolution have focused on the South Atlantic, but have usually been restricted to South America (Gan and Rao, 1991, 1994; Mendes et al, 2010; Vera et al, 2002; Reboita et al, 2010a) or individual case studies (Seluchi and Saulo, 1998; Funatsu et al, 2004; Piva et al, 2008, 2010, 2011; Iwabe et al, 2011; Dias Pinto and Da Rocha, 2011; Dias Pinto et al, 2013; Gozzo and da Rocha, 2013; Dutra et al, 2017). These studies provide insights into the development of cyclones in South America but do not provide a climatological view of the forcing mechanisms acting on cyclones over the South Atlantic Ocean.

The primary aim of this work is to produce a new climatology of cyclones in the South Atlantic region that can provide new insights into the conditions leading to genesis in different regions of the South Atlantic. Considering the large latitude range and the seasonal variability of cyclogenesis in the South Atlantic science questions addressed in this paper are:

- What are the main forcing mechanisms that control cyclone development in each genesis region of the South Atlantic in their most active season?
- Are there any differences in the genesis precursors and structures of intense cyclones that originate in distinct genesis regions?

The answers to these questions will not only confirm the traditional perspectives of South Atlantic cyclones (e.g., track and genesis density) but also the spatial distribution and genesis characteristics of South Atlantic cyclones

114 through composites of samples of cyclones as already performed for North  
115 Atlantic cyclones by Dacre and Gray (2009) and Catto et al (2010).

116 The paper continues in section 2 with a description of the data and method-  
117 ology used and the challenges of tracking cyclones over the South American  
118 continent. In section 3 the cyclone density statistics are discussed including  
119 the spatial distribution of cyclone characteristics at genesis time in section 4  
120 and the cyclone structure composites in section 5. Finally, a summary and  
121 final remarks are made in section 6.

## 122 2 Data and Methods

123 In order to answer the scientific questions, cyclones will be directly identified  
124 and tracked in data from a modern reanalysis with the tracks then synthesized  
125 into statistical diagnostics for further analysis of their distribution and prop-  
126 erties. The composites of the cyclone structure will also be done to provide a  
127 better understanding of cyclone genesis precursors for each region of interest.

### 128 2.1 Datasets

129 For this study, we used 32 years (1979-2010) of 6 hourly data from the Climate  
130 Forecast System Reanalysis produced by the National Centers for Environ-  
131 mental Prediction (NCEP CFSR; Saha et al, 2010). The NCEP-CFSR is an  
132 improvement on its older predecessors, NCEP-NCAR and NCEP-DOE, also  
133 produced by NCEP in terms of model formulation and resolution and data  
134 assimilation. The NCEP-CFSR includes coupled atmosphere, ocean, and land  
135 models, an interactive sea-ice model, assimilation of satellite radiances, and  
136 a significant increase in horizontal and vertical resolution of the atmospheric  
137 spectral model compared to the earlier NCEP reanalyses (Saha et al, 2010).

138 The atmospheric component is the Global Forecast System (GFS; Saha  
139 et al, 2010), which is a spectral model with a resolution of T382 (38 km) with  
140 64 hybrid vertical levels extending from the surface to 0.26 hPa. The ocean  
141 model is the Geophysical Fluid Dynamics Laboratory (GFDL) Modular Ocean  
142 Model version 4 (MOM4; Griffies et al, 2004) with 40 vertical levels and a zonal  
143 resolution of  $0.5^\circ$  and a meridional resolution of  $0.25^\circ$  between  $10^\circ\text{N}$  and  $10^\circ\text{S}$   
144 that gradually increases to  $0.5^\circ$  poleward of  $30^\circ\text{N}$  and  $30^\circ\text{S}$ . The NOAA land  
145 model (Ek et al, 2003) includes four soil layers and the ice model (Griffies  
146 et al, 2004) has two layers to account for variations below the surface.

147 Studies have shown that the latest set of reanalyses is a significant im-  
148 provement over earlier reanalyses (e.g., Saha et al, 2010; Hodges et al, 2011;  
149 Stopa and Cheung, 2014), especially in the Southern Hemisphere. New data  
150 assimilation techniques and new sources of observational data (e.g., satellite,  
151 ARGO floats) have played an enormous role in the better representation of  
152 atmospheric features of regions where the observational network previously  
153 had poor coverage, such as in the SH.

154 Stopa and Cheung (2014) showed that NCEP-CFSR represents global wind  
155 patterns in agreement with observed seasonal variability from buoy data and  
156 satellite products. These authors also recommend the use of the NCEP-CFSR  
157 for extreme event analysis. While other reanalyses underestimate extreme  
158 events, the NCEP-CFSR tends to overestimate them. Moreover, NCEP-CFSR  
159 was evaluated by Hodges et al (2011) in a study of extratropical cyclones. They  
160 compared four reanalyses regarding their ability to represent genesis and track  
161 density, maximum intensity and surface structure of extratropical cyclones.  
162 The ERA-Interim (ECMWF) and NCEP-CFSR have similar results, espe-  
163 cially representing cyclogenesis associated with orography. The NCEP-CFSR  
164 also shows the most intense systems, which reinforces the findings from Stopa  
165 and Cheung (2014).

## 166 2.2 TRACK Algorithm

167 The tracking of cyclonic features is performed using the automated tracking  
168 system, TRACK, of Hodges (1994, 1995) using the relative vorticity field at  
169 850 hPa computed from the U and V winds. Usually, surface cyclone tracking  
170 is done using mean sea level pressure (MSLP; e.g., Murray and Simmonds,  
171 1991) but, the relative vorticity permits the detection of weak and fast moving  
172 synoptic systems that can be masked by the background flow when using  
173 MSLP (Sinclair, 1994). Between 40°S and 20°S, the surface pressure gradient  
174 is strong and cyclones may not have a closed isobar until they reach higher  
175 latitudes or intensify. Because of this, the use of relative vorticity also allows  
176 the detection of the cyclones in their earlier stages, when a closed isobar is not  
177 present (Sinclair, 1994). For these reasons, to consider cyclones in the South  
178 Atlantic sector the use of vorticity may be a better choice rather than MSLP,  
179 as discussed by Sinclair (1994) and Hoskins and Hodges (2002).

180 Although vorticity has been selected for this study, it contains much small  
181 scale structure at the resolution of NCEP-CFSR which can cause problems of  
182 coherence when attempting to track features at the synoptic scale. However,  
183 the vorticity can be filtered to reduce the small spatial scales and focus on  
184 the synoptic scales to avoid problems during the identification process and  
185 tracking. The vorticity is spectrally filtered by converting to the spectral rep-  
186 resentation and truncating to T42 and tapering the spectral coefficients to  
187 smooth the data. The large-scale background is also removed by setting to-  
188 tal wavenumbers  $\leq 5$  to zero. For more details of the filtering see Hoskins  
189 and Hodges (2002). Cyclones are identified by determining the local minima  
190 (cyclones have negative vorticity in the SH) on a polar stereographic projec-  
191 tion, which is important to prevent a latitudinal bias (Sinclair, 1997), that are  
192 less than a threshold of  $-1.0 \times 10^{-5} s^{-1}$ . The locations are refined by deter-  
193 mining the off-grid locations using B-spline interpolation and steepest descent  
194 minimization, which results in smoother tracks.

195 The tracking is performed by first initializing a set of tracks by linking  
196 the detected feature points into tracks using the nearest neighbor method.

197 The tracks are refined by minimizing a cost function for the track smoothness,  
 198 which operates both forwards and backwards in time, subject to adaptive con-  
 199 straints on the maximum displacement in a time step and the track smoothness  
 200 (Hodges, 1999). Only systems that last longer than 24 hours (4 time-steps)  
 201 and have displacement from start to end greater than 1000 km are considered  
 202 for further analysis. The use of the 24 hours lifetime threshold rather than 48  
 203 hours was based on previous regional studies of the Southwestern South At-  
 204 lantic Ocean (e.g., Reboita et al, 2009; Reboita et al, 2018; Krüger et al, 2012).  
 205 Reboita et al (2009) showed that most cyclones in this area exist between 1-2  
 206 days, as well as when only intense cyclones are considered [ $\zeta \leq -2.5 \times 10^{-5} \text{ s}^{-1}$ ,  
 207 10-m wind vorticity]. Even with the short lifetime, these systems can promote  
 208 strong winds, which are important for wave generation and precipitation.

### 209 2.3 Validation and applied constraints

210 The tracking constraints adopted here differ from those used by Hoskins and  
 211 Hodges (2002) and are presented in Table 1. The tracking results were com-  
 212 pared to the synoptic charts from the Brazilian Navy from the summer (DJF)  
 213 and winter (JJA) of 2005. Manual analysis was done to see if the algorithm  
 214 captured cyclonic systems that influence the South American coast during the  
 215 above period. However, it is important to be aware that a direct comparison  
 216 between MSLP synoptic charts and the relative vorticity automated method  
 217 will not necessarily have a one to one correspondence due to the different na-  
 218 ture of the fields, as already discussed in section 2.2 (Sinclair, 1997; Hoskins  
 219 and Hodges, 2002).

220 The narrow shape of South America south of  $30^\circ$  allows the algorithm  
 221 with the standard settings for extra-tropical cyclones to connect some tracks  
 222 coming from the Pacific with tracks in the South Atlantic. The spurious tracks  
 223 crossing Andes Cordillera, remove genesis events of cyclones that develop near  
 224 the Eastern South American coast, between  $40^\circ\text{S}$  and  $20^\circ\text{S}$ . We solve this  
 225 issue by adding a rectangular region over the Andes, where the cyclones are  
 226 restricted to have a maximum displacement of  $1^\circ$  (geodesic) in one-time step  
 227 (Table 1). In this way, a cyclonic feature on the west side of South America  
 228 cannot be linked with a feature on the east side of the Andes in the next time  
 229 step, because the distance between the two features is larger than  $1^\circ$ . Also,  
 230 we reduce the maximum displacement to  $4^\circ$  per time step between  $30^\circ\text{S}$  and  
 231  $20^\circ\text{S}$  to inhibit the connection between thermal lows above the continent with  
 232 cyclogenesis at the coast.

233 Finally, we relax the constraints that allow changes in velocity (speed and  
 234 direction) for slow moving systems to include in the tracking some cyclones  
 235 at the Southeastern South American coast that present a quasi-stationary be-  
 236 havior at some stages of their lifecycle or abrupt change in their propagation  
 237 direction (Dias Pinto et al, 2013; Dutra et al, 2017). These slow moving sys-  
 238 tems spend some days close to the coast before they propagate southeastward,  
 239 causing strong winds and precipitation on the continent. During the validation

**Table 1** Adaptive constraints used by Hoskins and Hodges (2005) and in the present work. The last column indicates the allowed maximum displacement per time-step in each zone

Zonal Upper-bound displacements			
	Longitude	Latitude	$d_{max}$ (degree)
Hoskins and	0 – 360	-90 – -20	6.5
Hodges 2005	0 – 360	-20 – 0	3.0
Present work	0 – 360	-90 – -45	6.5
	0 – 285	-45 – -30	6.0
	285 – 295	-45 – -30	1.0
	295 – 360	-45 – -30	6.0
	0 – 360	-30 – -20	4.0
	0 – 360	-20 – 0	3.0

240 process, a set of tests was performed to find the configuration that best solves  
 241 these problems without interfering with the algorithm performance. This new  
 242 setup provided an 89% agreement with the synoptic chart analysis.

#### 243 2.4 Diagnostics

244 The spatial statistics are produced by the TRACK code using the spherical  
 245 kernel method (Hodges, 1996). The cyclogenesis density is computed using the  
 246 starting point of each track, excluding the tracks that start at the first time  
 247 step of the analysis period. In the same way, lysis density is calculated using  
 248 the end point of the track and do not consider tracks that end in the last time  
 249 step of the analysis period. Track density is computed using a single point  
 250 from each track closest to the estimation points. The raw density statistics are  
 251 scaled to number densities per month per unit area. The area unit is equivalent  
 252 to a  $5^\circ$  spherical cap, which is approximately  $10^6 km^2$ .

253 Besides the traditional statistics, other meteorological fields were added  
 254 to the tracks to provide more information about the genesis environment, life  
 255 cycle characteristics and vertical structure of the identified cyclones. This ad-  
 256 ditional information can be added by searching for a maximum, minimum  
 257 or average value within a radius from the tracked center at each time step.  
 258 Statistical diagnostics are computed from these additional fields in terms of  
 259 histograms and spatial distributions at a given time (e.g., maximum inten-  
 260 sity). The spatial distributions of genesis characteristics have been produced  
 261 by averaging the genesis characteristics (e.g., MSLP) of all cyclones generated  
 262 within a  $10^6 km^2$  area.

263 The first additional fields added to the tracks are the MSLP and the max-  
 264 imum wind speed at 925 hPa for the evaluation of the mean and maximum  
 265 intensity of the cyclones. Both fields are available in NCEP-CFSR and, no  
 266 further calculation was required. The minimum MSLP was sampled within a  
 267 radius of  $5^\circ$  (geodesic) from the tracked center and the maximum wind speed  
 268 at 925 hPa within a radius of  $6^\circ$ . Another way to measure intensity is using

the precipitation associated with the cyclone, which was computed as an area average within  $6^\circ$  using the NCEP-CFSR precipitation.

Other fields were added to the tracks to analyze further the cyclone development characteristics, all of them averaged within  $5^\circ$  of the cyclone centers. These additional fields are the mean upper-level jet velocity to evaluate upper-level atmospheric environments and the sea surface temperature gradient, static and conditional stability and integrated specific humidity to analyze the lower level atmospheric environment. The mean upper-level jet velocity was obtained through a weighted vertical average of velocity at each level between 100 and 500 hPa. The vertical stabilities and integrated humidity were computed using the layers between 1000 hPa and 700 hPa. The static stability was estimated by the potential temperature lapse-rate ( $\Gamma = \frac{\delta\theta}{\delta p}$ ), while conditional stability was obtained using the equivalent potential temperature lapse-rate ( $\Gamma_e = \frac{\delta\theta_e}{\delta p}$ ), where  $\theta_e$  is computed using the formulation of Bolton (1980).

## 2.5 Compositing of cyclones structure

To study the structure of the cyclones, compositing of the 30% most intense cyclones from each cyclogenesis region were considered to produce a more homogeneous group regarding their evolution. The cyclogenesis regions are defined through the genesis density distributions that are presented in section 3.2 and the intensity threshold applied to identify the most intense cyclones is discussed in section 5.

The compositing method used here was first used by Bengtsson et al (2007) to study tropical cyclone structure. After that, several works applied the same method to study extratropical cyclone structures (Bengtsson et al, 2009; Catto et al, 2010; Hodges et al, 2011; Dacre et al, 2012). This method consists of sampling the required field (e.g., MSLP,  $\theta_e$ ) using a radial grid centered at the cyclone center for each time step along its track. The radial grid is of a size 20-degree radius with a 0.5-degree grid spacing, both azimuthally and radially. The composites are produced by averaging the fields on the radial grid at each offset time relative to the genesis (the first point where the cyclone was detected). In previous works, the grid is rotated according to the cyclone propagation direction, what allows the system-relative winds to be analysed (e.g., air-flows inside the cyclone). However, this step was not adopted here because a non-rotated grid allows an assessment of the features relative to geographic coordinates and features that impact genesis that is relevant to the study of genesis precursors in South America. Times earlier than cyclogenesis are also considered to analyze the dynamic and thermodynamic features that lead to genesis. If the time of interest is before the time of genesis, the sampling was made using the position of the cyclone at the genesis time applied at the earlier time.

Besides the traditional meteorological fields (e.g., sea level pressure, geopotential), other derived fields were used for the compositing. The variables were calculated on a hemispheric grid ( $0^\circ$ - $90^\circ$ S) for each time step before being sam-

312 pled for the compositing. The relative humidity is estimated for a given tem-  
 313 perature, mixing ratio, and pressure, using a look-up table procedure (Murray,  
 314 1967). The vertically integrated moisture flux convergence (VIMFC) is used  
 315 as a measure of the lower tropospheric forced lifting. In this study, the VIMFC  
 316 is defined as the horizontal moisture flux convergence integrated between 1000  
 317 hPa and 700 hPa:

$$VIMFC = -\frac{1}{g} \int_{700hPa}^{1000hPa} \left( \frac{\partial uq}{\partial x} + \frac{\partial vq}{\partial y} \right) dp \quad (1)$$

318 where  $g$  is the gravitational acceleration,  $u$  and  $v$  are the zonal and merid-  
 319 ional component of the velocity, respectively, and  $q$  is specific humidity. Also,  
 320 the vertically integrated moisture transport (VIMT) was computed in a similar  
 321 way

$$\overrightarrow{VIMT} = -\frac{1}{g} \int_{700hPa}^{1000hPa} \left( uq \vec{i} + vq \vec{j} \right) dp \quad (2)$$

322 The VIMT has zonal and meridional components. The temperature advec-  
 323 tion at 850 hPa and the mass divergence at 200 and 300 hPa were computed  
 324 using centered finite differences for the partial derivatives. The potential vor-  
 325 ticity (PV) at 300 hPa was computed on isobaric levels ( $p$ ) on a global grid,  
 326 following Bluestein (1992) (page 264, Eq. 4.5.93).

### 327 3 Cyclone density statistics

328 In this section, the spatial statistics are first considered to provide information  
 329 on the general distribution of the cyclones and their seasonal variation. These  
 330 statistics provide us with the typical cyclogenesis regions within the South  
 331 Atlantic, which is going to be used as a guide to understanding differences in  
 332 genesis environment and structure of cyclones in the domain.

#### 333 3.1 Track Density

334 The cyclone track density is shown in Figs.1a and b for the austral sum-  
 335 mer (DJF) and winter (JJA), respectively. This shows there is a region of  
 336 maximum track density extending from west to east between 40°S and 55°S  
 337 [ $>10$  cyclones  $(10^6 km^2)^{-1} (month)^{-1}$ ] which extends over a larger latitudinal  
 338 range in the austral winter (JJA) than in the summer (DJF), this is the main  
 339 South Atlantic storm track. There is also a secondary track density region  
 340 [ $>6$  cyclones  $(10^6 km^2)^{-1} (month)^{-1}$ ] extending southeastward from Uruguay  
 341 and the South Brazilian coast, which seems to merge with the main southern  
 342 storm track. This second storm track is considered to be a subtropical branch  
 343 of the South Atlantic storm track (e.g., Hoskins and Hodges, 2005). During

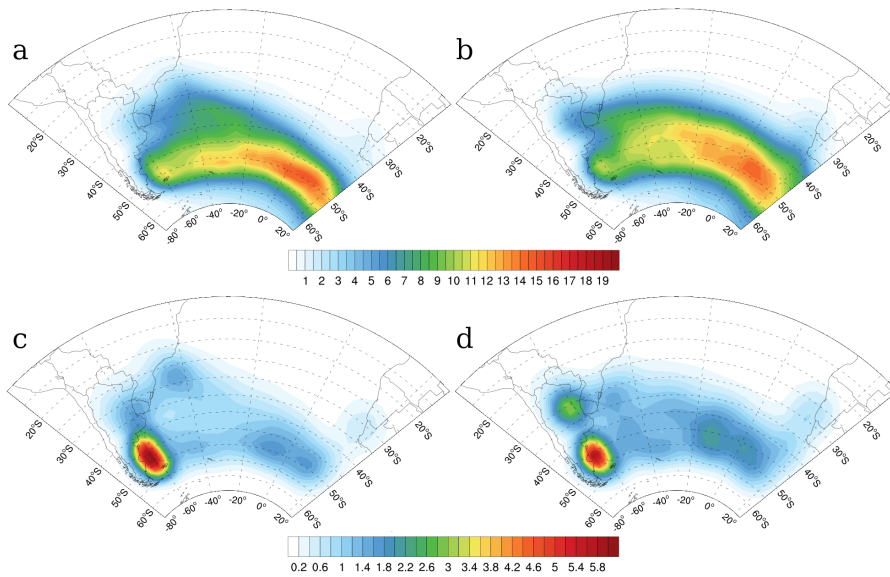


**Fig. 1** The cyclone track density for the (a) summer (DJF) and (b) winter (JJA), and the genesis density for the (c) summer (DJF) and (d) winter (JJA). The densities are computed using only cyclones with the first time step within South Atlantic domain, in a box between  $15^{\circ}\text{S}$ - $55^{\circ}\text{S}$  and  $75^{\circ}\text{W}$ - $20^{\circ}\text{E}$ . The density unit is cyclone per  $10^6 \text{ km}^2$  per month.

344 the summer, this branch originates more northward ( $30^{\circ}\text{S}$ ), while during the  
 345 other seasons it starts between  $30^{\circ}\text{S}$  and  $35^{\circ}\text{S}$ .

346 The pattern of track density and its variability throughout the year cor-  
 347 responds to that found in other studies (e.g., Taljaard, 1967; Sinclair, 1994;  
 348 Hoskins and Hodges, 2005). However, there are some differences between stud-  
 349 ies associated with some studies using relative vorticity and studies based on  
 350 MSLP or any field computed from the MSLP, e.g., geostrophic vorticity. For  
 351 example, Simmonds and Keay (2000) found that in the South Atlantic Ocean  
 352 sector the highest track density was around  $60^{\circ}\text{S}$  with no clear evidence of a  
 353 subtropical storm track in their results. These differences are related to using  
 354 MSLP to perform the cyclone tracking where the cyclones in the sub-tropics  
 355 are weak and fast moving, and often do not have a closed isobar in their  
 356 early stages due to the strong background pressure gradient at this location  
 357 (Sinclair, 1994, 1995, 1997; Hoskins and Hodges, 2005).

### 358 3.2 Genesis Density

359 Figures 1c and d show the genesis density of cyclones originating in the South  
 360 Atlantic domain in austral summer and winter respectively. There are three  
 361 regions of high genesis along the South American East coast: the central  
 362 Argentina coast between  $55^{\circ}\text{S}$  and  $40^{\circ}\text{S}$  (ARG, hereafter); Northeastern Ar-

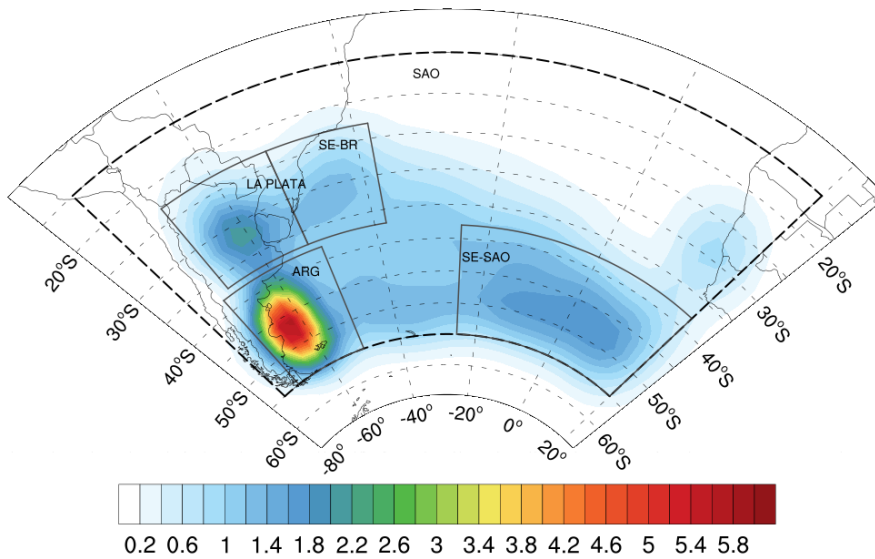


**Fig. 2** Genesis density for South Atlantic domain (marked in dashed gray line) computed for the entire period of 1979-2010. The four genesis regions are marked in black line. The density unit is cyclone per  $10^6 km^2$  per month.

363 gentina and the Uruguay region, close to the La Plata river discharge at  $30^\circ S$   
 364 (LA PLATA, hereafter), and the South-Southeast coast of Brazil, between  
 365  $30^\circ S$  and  $25^\circ S$  in the summer and  $35^\circ S$  and  $30^\circ S$  in the winter (SE-BR, here-  
 366 after). A fourth genesis region can be seen in the Southeastern South Atlantic  
 367 Ocean (SE-SAO, hereafter), centered at  $45^\circ S$  and  $10^\circ W$ . Both the cyclo-  
 368 genetic regions at  $50^\circ S$  and  $45^\circ S$  are active throughout the year. Despite that,  
 369 the ARG region presents slightly more genesis in summer and the SE-SAO in  
 370 winter. A see-saw behavior is noted at the northward latitudes too. The LA  
 371 PLATA region has more genesis in winter while the SE-BR genesis region is  
 372 active in summer. The four main cyclogenesis regions that exist in the South  
 373 Atlantic domain were selected based on the genesis density distribution, even  
 374 if a genesis regions present high genesis density values only in one analyzed  
 375 season. Figure 2 indicates the chosen sampling genesis regions. These regions  
 376 are based on the genesis density computed for the whole 1979-2010 period  
 377 and the boxes do not change according to the season. It is possible to note  
 378 another high genesis density region along the western coast of South African  
 379 and southern coast of Namibia, which is more intense during the winter. This  
 380 cyclogenetic area is also reported by Hoskins and Hodges (2005) and, accord-  
 381 ing to Inatsu and Hoskins (2004), it is driven by the South African Plateau.  
 382 However, the genesis density in western South Africa is weak compared with  
 383 the other regions described above, and it is not going to be included in this  
 384 study.

**Table 2** Total number of cyclogenesis events, annual mean and standard deviation for South Atlantic domain (15°S-55°S, 75°W-20°E) and in each preferred genesis region within the domain. The values were computed for the entire analysis period (1980-2010), summer (DJF) and winter (JJA).

region	1980 2010		DJF		JJA	
	total	annual mean	total	annual mean	total	annual mean
South Atlantic	12754	411.4 ± 10.2	2950	95.2 ± 6.4	3476	112.1 ± 7.6
SE-BR	856	27.6 ± 2.2	227	7.3 ± 1.9	201	6.5 ± 2.4
LA PLATA	1157	37.3 ± 3.1	224	7.2 ± 2.2	351	11.3 ± 3.0
ARG	2972	95.9 ± 4.6	831	26.8 ± 4.0	712	23.0 ± 4.5
SE-SAO	3666	118.3 ± 5.8	804	25.9 ± 4.1	1081	34.9 ± 5.6

385 Table 2 shows the number of genesis events for each defined region per  
386 season. The ARG and SE-SAO region are together responsible for 50% of  
387 genesis within the South Atlantic Ocean. Both of them are located in the  
388 main storm track latitude zone (Figs.1a and b). Looking at the number of  
389 cyclones in each region in different seasons it is possible to see that there is  
390 no strong seasonal variability in some regions, such as SE-BR and ARG. In  
391 fact, these two regions have less than 20% more cyclones in summer than in  
392 the winter. Through the genesis density map, the SE-BR region seems to be  
393 more concentrated northward of 30°S in the summer giving the idea of more  
394 genesis. For the LA PLATA and SE-SAO regions, there is a significant increase  
395 of genesis in the winter of 56% and 34.5% of cyclones, respectively. Regarding  
396 the differences in cyclone identification and tracking methods described above,  
397 it is difficult to compare the seasonal variability of genesis in specific regions  
398 from other studies as these have used different region boundaries to compute  
399 such variability (e.g., Reboita et al, 2010a).

400 The pattern of genesis densities compares well with those produced by  
401 other studies (Hoskins and Hodges, 2005; Reboita et al, 2010a; Hodges et al,  
402 2011). The SE-SAO region is within the main South Atlantic storm track  
403 though has not often been discussed in previous studies. Hoskins and Hodges  
404 (2005) included the storm path originating from this region showing that SE-  
405 SAO is located at the end of the storm path from the eastern South American  
406 coast suggesting a downstream development in this region. Trenberth (1991)  
407 and Berbery and Vera (1996) studied the SH storm track using an Eulerian  
408 approach and also found evidence of cyclone development in this region.

409 The differences in the magnitudes of genesis between this work and some  
410 previous studies (e.g., Gan and Rao, 1991; Sinclair, 1994, 1995; Hoskins and  
411 Hodges, 2005; Reboita et al, 2010a; Mendes et al, 2010) can be generally ex-  
412 plained by the field used to do the tracking, the feature identification thresh-  
413 olds (e.g., lifetime, minimum intensity), the method used to compute the  
414 statistics and even by the resolution of the data used. Gan and Rao (1991)  
415 and Mendes et al (2010) produced genesis density maps based on cyclone  
416 identification using the MSLP with manual and automated tracking meth-  
417 ods, respectively. Both of them found two main cyclogenesis regions on the

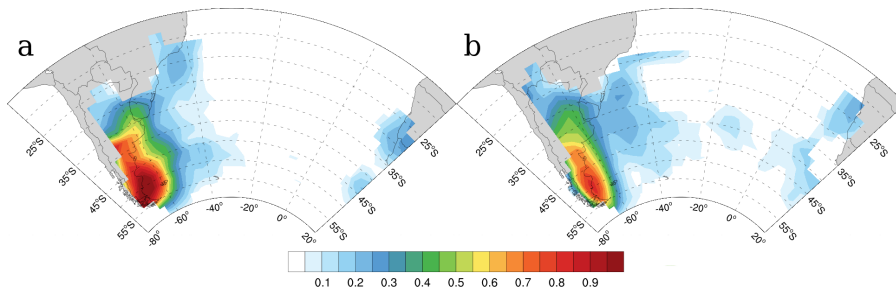


**Fig. 3** Mean growth rate ( $10^{-5} s^{-1} day^{-1}$ ) for the (a) summer (DJF) and (b) winter (JJA) computed using only cyclones with the first time step within South Atlantic domain, in a box between  $15^{\circ}S$ - $55^{\circ}S$  and  $75^{\circ}W$ - $20^{\circ}E$ .

418 South American coast equivalent to the LA PLATA and ARG genesis region  
 419 of this work. Sinclair (1995) and Hoskins and Hodges (2005) using methods  
 420 based on relative vorticity found a third region at  $25^{\circ}S$ , suggesting that cy-  
 421 clones developing in the SE-BR region were weak systems that may not be  
 422 detected by the use of MSLP as discussed earlier. There are also differences  
 423 between studies based on vorticity computed from the winds at a tropospheric  
 424 level above the boundary layer, e.g., 850 hPa (this study, Hoskins and Hodges,  
 425 2005) and those based on computing vorticity from 1000 hPa geopotential or  
 426 MSLP (e.g., geostrophic vorticity Sinclair, 1994, 1995). Although weak and  
 427 fast moving systems from subtropical latitudes are presented in the cycloge-  
 428 nesis distribution maps of Sinclair (1994, 1995), there is an underestimation  
 429 when compared with this work and other studies based on relative vorticity  
 430 from winds (Hoskins and Hodges, 2005; Reboita et al, 2010a). Reboita  
 431 et al (2010a) used vorticity from winds at 10 m, and an intensity threshold of  
 432  $-1.5 \times 10^{-5} s^{-1}$  and considered only cyclones with the first time point of the  
 433 track above the ocean. These authors found three genesis regions along the  
 434 South American coast, similar to our finding, although the regions above the  
 435 continent (LA PLATA) appears shifted to the coast at  $35^{\circ}S$ . The comparison  
 436 between Hoskins and Hodges (2005) and this study shows higher correspon-  
 437 dence, probably due to the same tracking method based on relative vorticity  
 438 of winds at 850 hPa albeit using different reanalyses. However, here, the mean  
 439 genesis density is higher in some locations when compared with Hoskins and  
 440 Hodges (2005). The genesis magnitude is much higher on the Argentina coast  
 441 and it is slightly higher in the SE-BR region for both seasons. The newly ap-  
 442 plied tracking constraints may be responsible for the accumulation of genesis  
 443 densities, although the shorter lifetime threshold is probably the main reason  
 444 for these differences. While we are using 24 hours, Hoskins and Hodges (2005)  
 445 considered tracks that last more than 48 hours. Comparing genesis densities  
 446 computed for cyclones that last more than 48h (not shown) with the results  
 447 in Figs. 1c and d, it is possible to see an increase in the genesis density in the  
 448 SE-BR and ARG regions, particularly in the summer, and in SE-SAO region.

449 It is important to note that here we define genesis as the first appearance of  
 450 the cyclone at low levels, i.e., the first point identified by the algorithm. Grise  
 451 et al (2013) argue that this definition may introduce some artificial features  
 452 into the genesis distribution, particularly on the lee side of mountain chains.  
 453 These authors deal with this issue by adding a minimum growth rate criteria  
 454 of  $2 \times 10^{-5} s^{-1} day^{-1}$  to select developing cyclones and showed that along  
 455 the U.S. Southeastern coast, over the Gulf Stream, the cyclone development is  
 456 greater than in the lee of the Rockies. Following Grise et al (2013) method, the  
 457 high genesis usually seen along the eastern side of the Rockies Mountains by  
 458 several authors (e.g., Hoskins and Hodges, 2002; Dacre and Gray, 2009) would  
 459 be a bias caused by the intersection of the 850 hPa level and the orography.  
 460 However, Fig.3, which shows the mean growth rate for the summer and winter,  
 461 shows that the maximum values occur on the lee side of Andes, in agreement  
 462 with the genesis density in Figs. 1c and d. The large values of mean growth  
 463 rate on the lee side enhance the evidence of genesis at this location rather  
 464 than a methodology issue. Moreover, Grise et al (2013) define genesis as a  
 465 developing phase, and their method allows a single cyclone to be counted  
 466 more than once in their density statistic if it has more than one developing  
 467 phase during its lifetime. This criterion may be useful to study fast growing  
 468 cyclones and intensification regions, but it may make it difficult to isolate the  
 469 precursor of a surface cyclone development in its earliest stages, as we aim in  
 470 this work.

### 471 3.3 Intensity, lifetime and duration if the cyclones

472 Figure 4 shows the histogram of relative vorticity from cyclones at their genesis  
 473 time for summer and winter in the South Atlantic region. The starting vorticity  
 474 of a cyclone may be important to estimate its impacts on the continent,  
 475 considering that three main cyclogenesis regions of the domain are located  
 476 near the coast and big cities. The frequency in Fig. 4 is displayed as a percent-  
 477 age to a better comparison between the genesis regions. The vorticity is scaled  
 478 by -1. **The SE-BR and LA PLATA cyclones present a similar distribution of**  
 479 **initial vorticity, with a peak between  $-2$  and  $-3 \times 10^{-5} s^{-1}$  in the summer,**  
 480 **corresponding to 36.5% and 42.9% of their systems, respectively. However, in**  
 481 **the winter, SE-BR cyclones present a big group of systems (20.0%) with ini-**  
 482 **tial vorticity between  $-4$  and  $-6 \times 10^{-5} s^{-1}$ . The ARG cyclones present less**  
 483 **intense cyclones at the time of genesis in the summer, being almost 44.3% of**  
 484 **its systems between  $-1$  and  $-2 \times 10^{-5} s^{-1}$ . The SE-SAO region has a higher**  
 485 **frequency of cyclones with higher intensity at genesis time in both seasons.**  
 486 **The majority of the South Atlantic cyclones have the starting cyclonic vor-**  
 487 **ticity weaker in summer than winter. The mean intensity at genesis time is**  
 488  **$-2.8 \pm 1.4 \times 10^{-5} s^{-1}$  in summer and  $-3.4 \pm 1.6 \times 10^{-5} s^{-1}$  in winter (Table 3). The**  
 489 **SE-SAO region has higher intensity at genesis time when compared to the**  
 490 **other regions, reaching a mean of  $-4.0 \pm 1.9 \times 10^{-5} s^{-1}$  during winter (Table 3).**  
 491 **The high initial vorticity of the SE-SAO region reinforces the idea of down-**

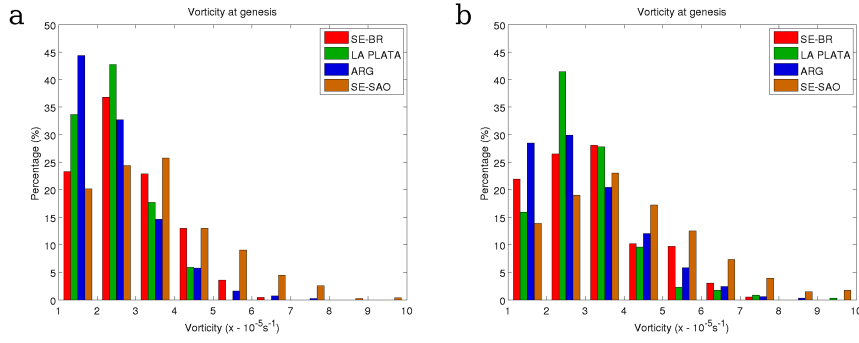


**Fig. 4** Histograms of the vorticity at the genesis time in the (a) summer and (b) winter for the cyclones which originate in SE-BR (red), LA PLATA (green), ARG (blue) and SE-SAO (orange) regions. The relative vorticity is scaled by  $-1 \times 10^{-5} s^{-1}$  and the y-axis shows the percentage computed based on the total number of cyclones detected in each defined genesis region.

492 stream development mechanisms (e.g., Orlanski and Katzfey, 1991) or other  
 493 secondary genesis mechanisms. The mean growth rate in the SE-SAO region  
 494 is weaker than in other genesis regions - only a weak signal in the winter in  
 495 Fig. 3 - which shows that the cyclogenesis in this region occurs associated with  
 496 a pre-existing cyclone. It is important to clarify that the location of the SE-  
 497 SAO region within the main South Atlantic storm track may lead to spurious  
 498 tracks as results of tracking issues related to the separation of one storm into  
 499 two separate storms. **This problem is more likely to occur within regions where**  
 500 **there are occluding cyclones. The South Atlantic domain presents low values of**  
 501 **cyclolysis density (when compared with genesis) and cyclone occlusion occurs**  
 502 **widespread across the basin, including the SE-SAO region, and concentrated**  
 503 **near Antarctica (not shown). Therefore, this problem could happen in any**  
 504 **location of the study domain and would not influence the genesis only in this**  
 505 **area.**

506 Table 3 contains the mean relative vorticity at genesis time, mean lifetime  
 507 and mean cyclone displacement speed in each defined genesis region computed  
 508 for the whole period, and separately for summer and winter. The mean life-  
 509 time of South Atlantic cyclones is longer in the summer ( $4.1 \pm 2.9$  days) than  
 510 in winter ( $3.7 \pm 2.4$  days). The region that presents the longest lifetime is the  
 511 LA PLATA region ( $5.4 \pm 2.9$  days in summer). The SE-SAO has the short-  
 512 est duration systems ( $3.4 \pm 2.4$  days) for the whole period. In general, South  
 513 Atlantic cyclones tend to be slightly faster in the winter ( $15.7 \pm 4.9 m s^{-1}$   
 514 against  $14.4 \pm 4.6 m s^{-1}$  in the summer). ARG and SE-SAO regions present  
 515 the highest displacement speed due to the large-scale flow dominated by the  
 516 westerlies. The mean values presented in Table 3 are higher when compared  
 517 with other South Atlantic climatologies. Reboita et al (2009), using 10 years  
 518 of NCEP-DOE (Kanamitsu et al, 2002), found a mean speed of  $11.0 m s^{-1}$ ,  
 519 a mean lifetime of 2.6 days and an initial vorticity of  $-2.5 \times 10^{-5} s^{-1}$ . These

**Table 3** The mean 850 hPa relative vorticity at genesis time (scaled by  $-1 \times 10^{-5} s^{-1}$ ), mean lifetime (days) and mean cyclone displacement speed ( $ms^{-1}$ ) and standard deviations computed within South Atlantic domain ( $15^{\circ}S-55^{\circ}S$ ,  $75^{\circ}W-20^{\circ}E$ ) and within each defined genesis region. The means were calculated for the whole analysis period (1980-2010), only for summer (DJF) and only for winter (JJA).

1980 - 2010			
region	initial vort.	lifetime	speed
South Atlantic	3.1±1.5	3.9±2.7	15.0±4.8
SE-BR	3.0±1.3	4.2±2.7	13.2±4.7
LA PLATA	2.7±1.1	5.3±3.1	12.6±3.8
ARG	2.7±1.2	4.0±2.6	14.9±4.0
SE-SAO	3.7±1.8	3.4±2.4	17.1±4.7
DJF			
region	initial vort.	lifetime	speed
South Atlantic	2.8±1.4	4.1±2.9	14.4±4.6
SE-BR	2.9±1.1	4.8±3.0	12.1±4.2
LA PLATA	2.4±0.9	5.4±2.9	12.2±3.7
ARG	2.4±1.1	4.3±2.9	14.5±3.9
SE-SAO	3.4±1.6	3.7±2.6	16.3±4.4
JJA			
region	initial vort.	life time	mean speed
South Atlantic	3.4±1.6	3.7±2.4	15.7±4.9
SE-BR	3.2±1.3	3.5±2.2	14.3±4.8
LA PLATA	3.0±1.2	5.1±3.0	13.1±3.9
ARG	3.0±1.4	3.7±2.2	15.2±4.1
SE-SAO	4.0±1.9	3.3±2.2	17.6±4.8

520 differences can be understood by the NCEP-DOE lower resolution, but also  
521 by the fact that in Reboita et al (2009) the cyclones are tracked based on the  
522 vorticity computed from the 10 m winds. The cyclone structure at the surface  
523 is affected by drag, and the winds are weaker when compared with the 850  
524 hPa field. Also, some disturbance can still be tracked at 850 hPa that do not  
525 exist at the surface, resulting in the longer lifetimes reported in Table 3.

526 Figures 5 and 6 shows histograms of different types of cyclone intensity  
527 measures computed as the lifetime maximum or minimum value within the  
528 South Atlantic domain, defined as SAO in Fig. 2. The histograms of maxi-  
529 mum intensity in terms of vorticity (Figs.5a and b) show that the cyclones  
530 from the LA PLATA region are the most intense within the South Atlantic  
531 Ocean, as also seen in terms of 925 hPa wind speeds (Figs.6a and b). This  
532 characteristic is less clearly seen when considering MSLP (Figs.5c and d), as  
533 this field is more likely to be influenced by the large scale background and  
534 tends to focus on larger spatial scales. However, the LA PLATA and SE-BR  
535 regions show a small peak of intense cyclones centered at 945 hPa in the winter  
536 for the MSLP. The vorticity maximum intensity distribution shows there are  
537 three peaks, indicating three groups of cyclones in the LA PLATA region. The  
538 first is between  $-3.5$  and  $-4.5 \times 10^{-5} s^{-1}$ , the second is around  $-9.5 \times 10^{-5} s^{-1}$ ,  
539 and a third peak around  $-13.0 \times 10^{-5} s^{-1}$ . They exist in both seasons, but  
540 in the winter their frequency is similar, showing an increase in more intense

541 cyclones in this season. In the MSLP histograms, there are two peaks for the  
542 LA PLATA cyclones in the summer, and three peaks in the winter, including  
543 the one centered around 945 hPa. The SE-BR region shows maximum vorticity  
544 around  $-4.5 \times 10^{-5} s^{-1}$  in the summer and between  $-2.5$  and  $-4.5 \times 10^{-5} s^{-1}$  in  
545 the winter, but the tail of the distribution shows an increase of strong systems  
546 in the winter. The similarity between the LA PLATA and SE-BR intensity  
547 distributions may be related to their proximity to each other, mainly in win-  
548 ter when these two regions are basically at the same latitude. Hence, they  
549 may have the same growth mechanisms that change according to the seasonal  
550 variability. The only difference is the presence of more weak systems in the  
551 SE-BR region, especially during winter. The cyclones from the ARG and SE-  
552 SAO regions have maximum intensity distributions similar to the distribution  
553 for cyclones from all of the South Atlantic. The distribution changes if the  
554 maximum intensity is considered to be within the South Atlantic Ocean or  
555 is outside the domain (not shown). Larger intensities for vorticity and MSLP  
556 are found if we take into account all track points instead of the point within  
557 the domain which is expected because cyclones that travel long distances and  
558 move poleward tend to become more intense (e.g., Hoskins and Hodges, 2005).  
559 The most affected distribution with the change of maximum intensity point  
560 selection is the SE-SAO region due to its proximity to the SAO domain bound-  
561 ary.

562 The histogram of maximum precipitation rate within the cyclone reveals  
563 that SE-BR and LA PLATA cyclones generate the most intense precipitation  
564 with a similar pattern (Figs.6 c and d). The cyclones in the ARG and SE-  
565 SAO regions show maximum precipitation distributions with fewer cyclones  
566 with precipitation above  $20 \text{ mm day}^{-1}$  when compared to cyclones from all  
567 the South Atlantic domain. According to the intensity histograms, cyclones  
568 from the SE-BR and LA PLATA regions are associated with intense winds  
569 and precipitation. Most of these systems have a lifecycle confined near the  
570 Southeastern American coast (not shown). This fact is particularly important  
571 as even with a small number of cases per year these cyclones impact the coastal  
572 region directly.

#### 573 **4 Spatial Distribution of cyclone properties**

574 The distribution of properties of South Atlantic cyclones is discussed in an  
575 attempt to understand the dynamical and thermodynamical spatial charac-  
576 teristics of cyclone development from a climatological point of view. Some of  
577 these distributions are shown as anomalies, computed as a deviation from the  
578 seasonal climatology.

579 The spatial distribution of the SST gradient at the time of genesis (Figs.7a  
580 and b) shows that between  $30^{\circ}\text{S}$  and  $45^{\circ}\text{S}$  cyclones develop in a high SST gra-  
581 dient environment (Sinclair, 1995; Hoskins and Hodges, 2005). Sinclair (1995)  
582 suggested that the correlation between high SST gradient and cyclogenesis  
583 may be related to the transfer of oceanic baroclinicity to the atmosphere.

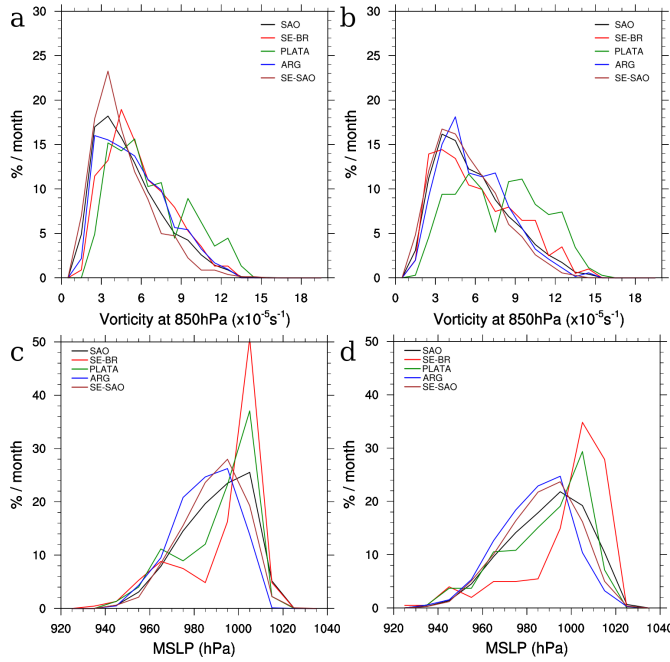


**Fig. 5** Histograms of the maximum filtered vorticity at 850 hPa in the (a) summer and (b) winter; and the MSLP (hPa) in the (c) summer and (d) winter, within South Atlantic domain. The vorticity is scaled by  $-1 \times 10^{-5} s^{-1}$  and the MSLP minima was searched within  $5^\circ$  radius from the center of the cyclone. The intensity histograms were produced for cyclones that originate in each genesis region separately. The percentage was computed based on the mean cyclones per month for each region: SE-BR (2.4), LA PLATA (2.4), ARG (8.9), SE-SAO (8.7) and for all South Atlantic domain (SAO; 31.72).

584 Comparing the track density (contours in Figs.7a and b) with the distribu-  
 585 tions of the SST gradient at the time of genesis it is possible to see that the  
 586 position of the main South Atlantic storm track are related to high values of  
 587 SST gradient at genesis time, as long as these high values are located on the  
 588 equatorward flank of the storm track. The development of cyclones along the  
 589 Southeastern South American coast appears to be associated with the pres-  
 590 ence of the high SST gradient environment that, in this location, is driven by  
 591 the variability of the Brazil-Malvinas Confluence (BMC) and its associated  
 592 fronts. During summer, the BMC is southward of its mean position affecting  
 593 lower troposphere baroclinicity in the ARG region. In winter the confluence  
 594 shifts northward reaching lower latitudes (Olson et al, 1988). Combined with  
 595 the BMC shift, there is a northward intrusion of the La Plata River ( $34^\circ S$ ) and  
 596 Patos Lagoon ( $32^\circ S$ ) discharge within the continental shelf off eastern South  
 597 America during winter (Piola et al, 2000). The result is a cool SST tongue over  
 598 the continental shelf that generates the subtropical shelf front (STSF) when  
 599 it encounters the warmer waters of the Brazil Current (Fig.7d; Campos et al,  
 600 1999; Piola et al, 2000). The STSF and the BMC position in the winter affect

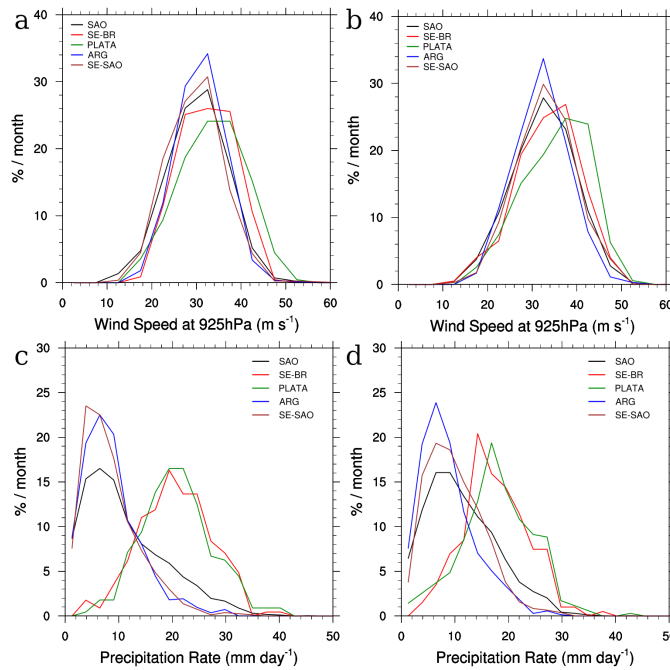


**Fig. 6** Histograms of the maximum wind speed at 925 hPa ( $m s^{-1}$ ) in the (a) summer and (b) winter; and the precipitation rate ( $mm day^{-1}$ ) in the (c) summer and (d) winter, within South Atlantic domain. The maximum wind speed at 925 hPa is searched within  $6^\circ$  radius from the center of the cyclone and the precipitation is averaged within a  $5^\circ$  radius. The intensity histograms were produced for cyclones that originate in each genesis region separately. The percentage was computed based on the mean cyclones per month for each region: SE-BR (2.4), LA PLATA (2.4), ARG (8.9), SE-SAO (8.7) and for all South Atlantic domain (SAO; 31.72).

601 the SST gradient at the time of genesis of the cyclones on the Southeastern  
 602 South American coast, at  $25^\circ S - 30^\circ S$  (Fig.7b). Moreover, even cyclones that  
 603 originate above the continent, in the LA PLATA region, are influenced by the  
 604 increase of low-level baroclinicity as long as they move toward the ocean after  
 605 genesis. The SST gradient at the time of genesis is weaker in SE-SAO, when  
 606 compared with the other regions, what is in agreement with the low values of  
 607 mean growth rate at this location (Fig. 3).

608 Figures 8a and b show the low level integrated humidity anomaly distribu-  
 609 tion at the time of genesis for the summer and winter, respectively. In both  
 610 distributions, the humidity anomalies are positive in most parts of the domain,  
 611 but mainly on the lee side of the Andes between  $25^\circ S$  and  $40^\circ S$  and in the  
 612 SE-BR region. These higher values of moisture at the time of genesis are a  
 613 consequence of an intensified moisture flux from the South American low-level  
 614 jet (SALLJ), on the eastern slope of the Andes, and from the South Atlantic  
 615 Subtropical High (SASH), towards the southeastern coast (Marengo et al,

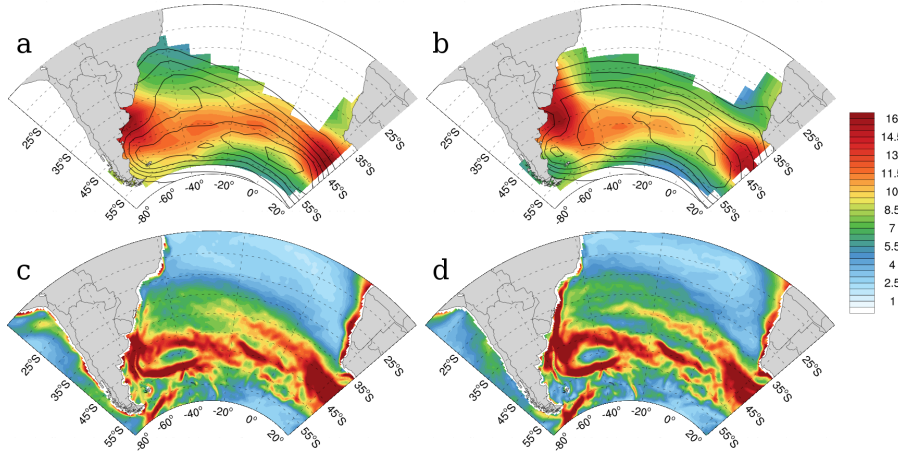


**Fig. 7** Spatial distribution of sea surface temperature (SST) gradient at the time of genesis (shaded) and track density (contours each 2 cyclones  $(10^6 km^2)^{-1} month^{-1}$ ) in the (a) summer and (b) winter. SST gradient climatology in South Atlantic Ocean in the (c) austral summer and (d) winter. The gradient unit is  $10^{-3} K km^{-1}$ . The fields are not plotted where genesis density  $< 0.2$  cyclones  $(10^6 km^2)^{-1} month^{-1}$ .

2004; Vera et al, 2006; Drumond et al, 2008). The positive moisture anomaly is more concentrated in the LA PLATA region in the winter, when the SASH southwestward position enhances the moisture transport to this location. Vera et al (2002) and Mendes et al (2007) have shown the importance of moisture transport from the tropics in the development of cyclones in the Southeastern South American coast. During cyclone development the warm and humid fluxes from the SASH feeds the cyclone, providing low-level instability.

The spatial distribution of the potential temperature ( $\theta$ ) and equivalent potential temperature ( $\theta_e$ ) lapse rates are considered here as a measure of atmospheric static stability and conditional stability, respectively. In this way, less (more) negative values of  $\delta\theta/\delta p$  mean a less (more) stable low-level atmosphere, and positive (negative) values of  $\delta\theta_e/\delta p$  mean a conditionally unstable (stable) low-level atmosphere. Here we used anomalies from the climatological field, which follow this idea, showing a less stable genesis environment with positive values. Figures 8c and d show the static stability anomaly in both winter and summer seasons. The static stability difference between the two seasons is bigger over the continent due to changes in the contrast between the lower atmospheric and land surface temperatures. The genesis environment over South American is less statically stable in the winter than in the summer, which may contribute to the greater genesis activity in LA PLATA in the winter. The SE-BR and ARG cyclones develop in a relatively statically unstable environment over the ocean. However, the ARG region presents a less statically stable environment during the summer. In the winter, the SE-BR regions have a more unstable genesis environment. The SE-SAO region shows a less stable environment in both season, but with some variation within its

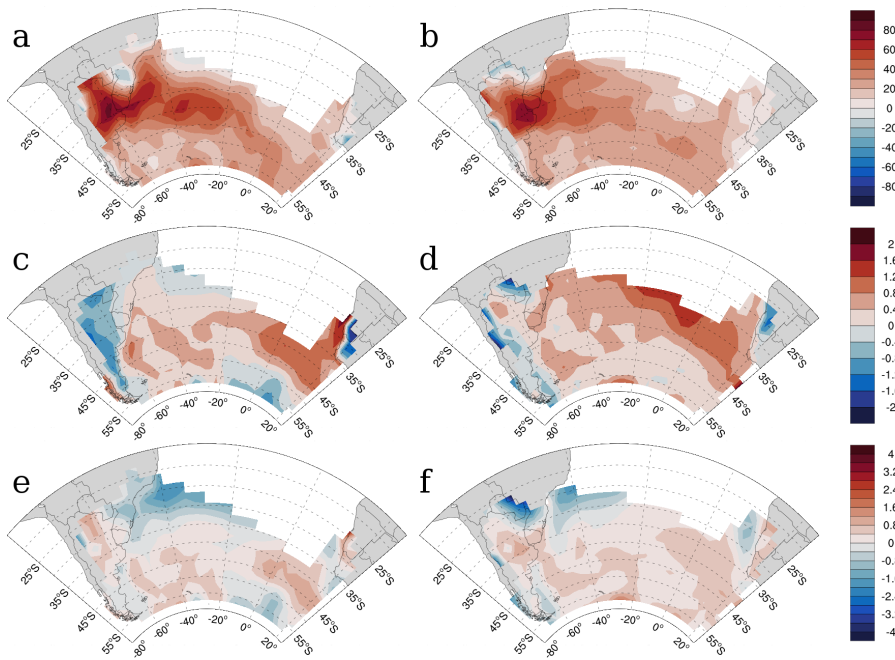


**Fig. 8** Spatial distribution of anomalies of the integrated humidity at lower-level ( $kg\ kg^{-1}$ ) at the time of genesis in (a) austral summer and (b) winter;  $\delta\theta/\delta p$  ( $10^{-2}\ K\ hPa^{-1}$ ) at the time of genesis in (c) summer and (d) winter, and;  $\delta\theta_e/\delta p$  ( $10^{-2}\ K\ hPa^{-1}$ ) at the time of genesis in (e) summer and (f) winter. The anomalies are computed using the season climatology and the fields are not plotted where genesis density  $< 0.2$  cyclones ( $10^6\ km^2$ ) $^{-1}\ month^{-1}$ .

641 domain (less stable in its northern edge). Figures 8e and f show the conditional  
 642 stability anomalies at genesis time. The LA PLATA cyclones develop in a less  
 643 convectively stable environment when compared to the climatology that may  
 644 be explained by the positive moisture anomaly at this location. Although the  
 645 SE-BR region presents a more stable environment (negative anomalies) this  
 646 region is conditionally unstable in the summer and has a neutral environment  
 647 in the winter. The reason why these cyclones show a less unstable environ-  
 648 ment at the time of genesis could be justified by the presence of previous  
 649 convection, where further evidence of this can be found through the cyclone  
 650 composite analysis in section 5. Over the ocean, including the SE-SAO region,  
 651 the genesis environment is less stable than the climatology in both seasons.

652 Finally, the distributions of the upper-level jet speed anomaly at the time  
 653 of genesis is shown in Figs.9a and b for summer and winter, respectively. The  
 654 mean upper-level jet for each season is also presented in Fig.9, where the jet is  
 655 defined when the speed is greater than  $20\ m\ s^{-1}$ . Cyclones tend to develop for  
 656 upper-level jets which tend to be more intense at the time of genesis than in  
 657 the mean climatology, as seen through the positive anomaly values over most  
 658 of the domain in both seasons. The only exception is the cyclones that form

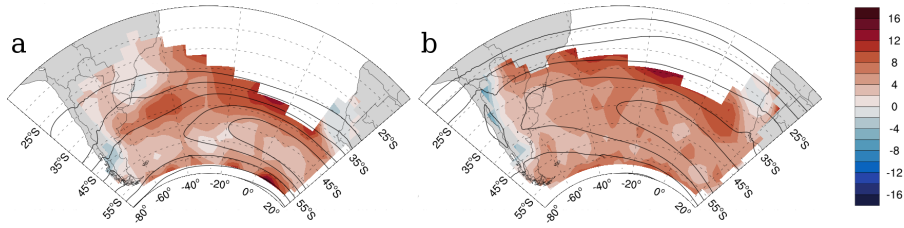


**Fig. 9** Spatial distribution of upper-level jet speed anomaly ( $m s^{-1}$ ) in austral (a) summer and (b) winter) at the time of genesis. The upper-level jet velocity is computed by the weighted vertical average at each level between 100 and 500 hPa. The anomalies are computed using the season climatology, which is contoured each  $4 m s^{-1}$  from  $20 m s^{-1}$ . The anomaly distribution at genesis are not plotted where genesis density  $< 0.2$  cyclones  $(10^6 km^2)^{-1} month^{-1}$ .

**Table 4** Intensity threshold (scaled by  $-1 \times 10^{-5} s^{-1}$ ) applied to the selection of 30% most intense cyclones of each defined genesis region in summer and winter and the number of cyclones used to compute each composite.

	DJF		JJA	
	threshold	number	threshold	number
SE-BR	7.1	61	8.8	44
LA PLATA	8.8	63	10.5	92
ARG	8.2	197	8.6	169
SE-SAO	8.9	167	10.0	221

659 over the SE-BR in the summer, that show a genesis environment with a weak  
 660 upper-level jet (Fig.9a). The weak upper-level jet may suggest that vertical  
 661 wind shear is not strong in this region and may indicate a subtropical genesis  
 662 environment (Gozzo et al, 2014).

## 663 5 Cyclone structure

664 In this section, the cyclone composites are presented to understand the cyclo-  
 665 genesis precursors of each defined genesis region. An intensity threshold was  
 666 used to select the strongest 30% of systems of each region in each season. As  
 667 discussed in section 3.3, the threshold for each region and season changes ac-  
 668 cording to its maximum intensity. Table 4 shows the limits adopted in each  
 669 case and the number of systems used in each composite. Figure 10 shows the  
 670 geographical position of the cyclone center used for the composites at 12 h  
 671 before, and at time of genesis for each region in both seasons.

672 First, an overview of the cyclone structure for each genesis region is ex-  
 673 amined to explore the general extratropical cyclone features at the time of  
 674 genesis. The cyclone structure for each region will be shown separately for  
 675 composites of time steps before and after the time of genesis. For clarity, only  
 676 composites at 12h before the time of genesis and 24h after the time of genesis

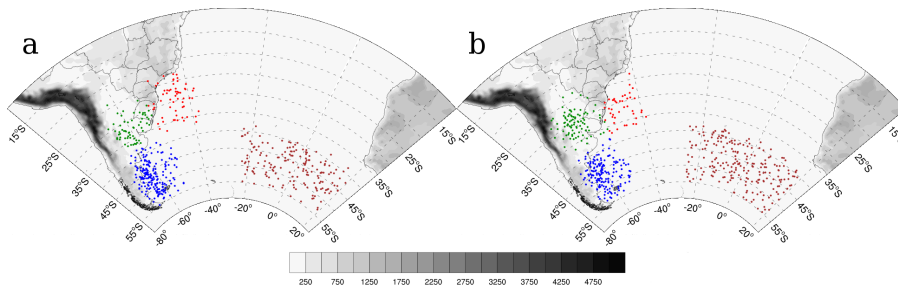


**Fig. 10** Map of orography ( $m$ ; shaded) and geographical positions of the cyclones used in the structure compositing in the (a) summer (DJF) and (b) winter (JJA). The dots denote the position of the cyclone center at the time of genesis, which is also the center position used to the composite at 12h before genesis time. The cyclones from each genesis regions are showed in different colors: SE-BR (red), LA PLATA (green), ARG (blue), and SE-SAO (brown).

677 time will be shown. The discussion of the intensification of the precursors is  
 678 considered in terms of the thermal advection at 850 hPa, geopotential height at  
 679 500 hPa, vertical velocity, vertically integrated moisture transport and mois-  
 680 ture flux convergence (1000 hPa - 700 hPa) and upper-level divergence and  
 681 geopotential (200 hPa).

## 682 5.1 General structure of cyclone genesis

683 The composite structure of  $\theta_e$  at 925 hPa and MSLP at the time of genesis  
 684 are shown in Fig.11. The cyclones from all genesis regions tend to form in a  
 685 temperature gradient zone with the warm isotherms folding towards the center,  
 686 following the conceptual models of Bjerknes et al (1922) and Shapiro and  
 687 Keyser (1990). As discussed before (section 2.2), the use of relative vorticity  
 688 in the cyclone tracking allows the identification of cyclonic features without a  
 689 closed isobar, as it is possible to see in most of the MSLP composites (Fig.11).  
 690 The MSLP composite structure also retains the position of the SASH relative  
 691 to the genesis region. In the SE-BR and LA PLATA regions, the SASH  
 692 signature in the MSLP mean field is east-northeastward of the cyclone center.

693 Figure 12 shows the composites of RH and PV at 300 hPa, and  $\theta_e$  at 925  
 694 hPa at the time of genesis. The RH structure in some composites shows a  
 695 horizontal elongated cloud band across the center. The presence of this cloud  
 696 band is usually related to a strong thermal gradient at the surface, indicating  
 697 frontal cloud. In general, this cloud band structure within an extratropical  
 698 cyclone is called polar front cloud and is associated with a high baroclinic  
 699 environment (Streten and Troup, 1973; Browning and Roberts, 1994). The  
 700 presence of a more pronounced cloud band at the time of genesis could be evi-  
 701 dence of secondary cyclogenesis (Dacre et al, 2012) and is observed in SE-BR  
 702 cyclones in the summer and SE-SAO cyclones in both seasons. The composite  
 703 of PV at 300 hPa shows an upper-level trough upstream of the cyclone cen-

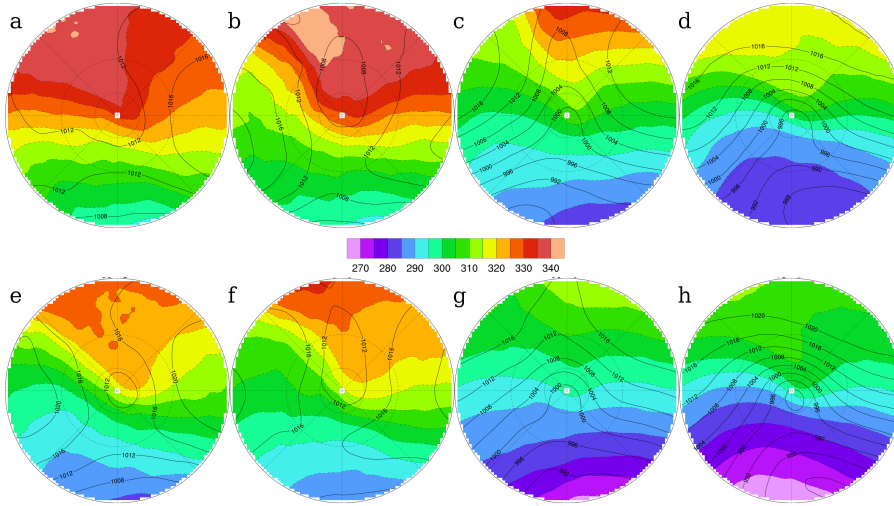


**Fig. 11** Composites of equivalent potential temperature ( $\theta_e$ ) at 925 hPa (K; shaded) and MSLP (hPa; black line) from different genesis regions in the summer (a-d) and winter (f-g): SE-BR (a,e) LA PLATA (b,f), ARG (c,g) and SE-SAO (d,h).

704 ter in all cyclones. The only exception is the SE-BR cyclones in the summer,  
 705 where the upper-level trough seems to be weak. The PV values of -2 PVU ( $1 \times 10^{-6} s^{-1}$ ) indicate a stratospheric intrusion upstream of the cyclone  
 706 development center, in the Southern Hemisphere. The PV values are higher in  
 707 cyclogenesis that occurs poleward due to the lower tropopause.  
 708

## 709 5.2 Cyclone structure evolution during genesis

### 710 5.2.1 Southeastern Brazilian Coast (SE-BR)

711 Figure 13 shows the composite of the surface temperature advection, winds at  
 712 850 hPa and geopotential height at 500 hPa for the SE-BR cyclones. In the  
 713 summer, the temperature advection is very weak before the time of genesis,  
 714 increasing slowly after genesis, and showing no evidence of strong frontal char-  
 715 acteristics. The winter composites show strong warm advection before genesis  
 716 and a rapid increase of cold and warm advection after the genesis time. The  
 717 low-level wind structure and MSLP at the time of genesis (Fig.11a and e)  
 718 show the southwestern portion of the SASH in the upper-east side of the com-  
 719 posites. The SASH is located northwestward of its main position during the  
 720 winter (e.g., Sun et al, 2017), which may reflect the stronger warm advection  
 721 before genesis. Moreover, there is strong low-level baroclinicity in the SE-BR  
 722 region due to the northward shift of the BMC and STSF in the winter. The  
 723 thermal advection associated with the ocean heat and moisture fluxes can act  
 724 to decrease the low-level stability contributing to the cyclone development. In

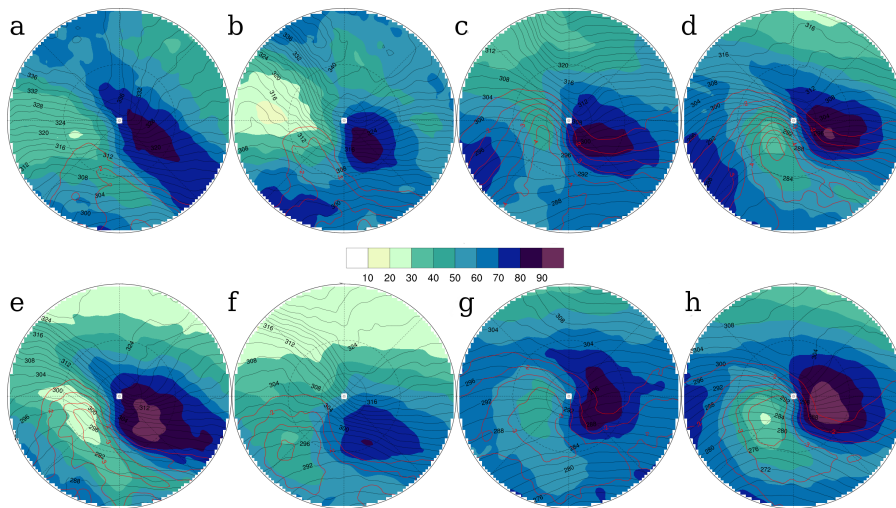


**Fig. 12** Composites of equivalent potential temperature ( $\theta_e$ ) at 925 hPa (K; black lines), RH (%) (shaded) and PV at 300 hPa (PVU; red line) from different genesis regions in the summer (a-d) and winter (e-g): SE-BR (a,e) LA PLATA (b,f), ARG (c,g) and SE-SAO (d,h).

725 both seasons there is a mid-level trough moving to the east that is located  
 726 westward of the cyclone center at the time of the genesis giving support to the  
 727 cyclone development. The vertical velocity at 700 hPa, the integrated moist  
 728 flux convergence and transport is shown in Fig.14. In the summer, there is  
 729 a narrow band of upward motion and moisture convergence with a NW-SE  
 730 orientation before the time of genesis. This feature in the summer composites  
 731 may indicate the presence of an “old” front, possibly generated by a “par-  
 732 ent” cyclone located southeastward from the genesis area. This can explain  
 733 the structure analogous of the “polar front cloud” observed for the RH at 300  
 734 hPa at the genesis time for the SE-BR summer composites (Fig.12a). The exist-  
 735 ence of this convergence strip associated with a cloud band at 300 hPa may be  
 736 indicative of secondary cyclogenesis. However, the relatively weak thermal ad-  
 737 vection leads us to believe that this type of secondary development occurs due  
 738 to the effects of moist deformation strain acting to decrease the frontal tem-  
 739 perature gradient of a preexisting front (e.g., Renfrew et al, 1997; Dacre and  
 740 Gray, 2006). Following the summer cyclone development, the mid-level trough  
 741 position seems to enhance the vertical movement. However, the proximity of  
 742 its axis to the cyclone center reveals a small tilt of the system (Fig.13c), which  
 743 does not totally explain the enhancement of the vertical movement. Figure 15  
 744 shows the divergence of the winds and geopotential at 200 hPa. The summer  
 745 composites show the weak upper-level trough that intensifies during the gene-  
 746 sis process (Fig.15b). The upper-level divergence is due to a diffluent flow and  
 747 gives support to the development of the cyclone at low level, enhancing vertical  
 748 velocity upwards and organizing the small cores of moisture convergence to a

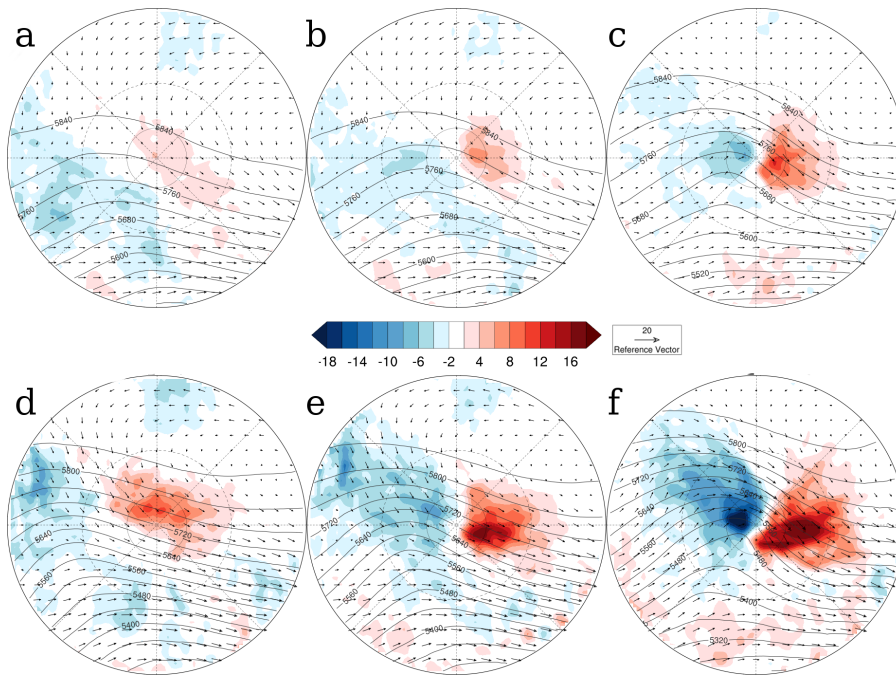


**Fig. 13** Composites of SE-BR cyclones temperature advection at 850 hPa ( $10^{-5} K s^{-1}$ ; shaded), geopotential height at 500 hPa (gpm; blue line) and winds at 850 hPa ( $ms^{-1}$ ) in the (a-c) summer and (d-f) winter: (a,d) at 12 hours before time of genesis; (b,e) at time of genesis, and; (c,f) at 24 hours after genesis.

749 larger region at the center of the cyclone at the time of the genesis (Figs.13b  
750 and 14b).

751 In the winter, the existence of a trailing front is not evident. Despite the  
752 presence of upward movement and low-level convergence, they seem to be  
753 promoted by the mid-level trough even before genesis (Figs.13d,e). The upper-  
754 level trough at 200 hPa promotes divergence downstream at the same location  
755 where there is low-level convergence and mid-level upward motion, showing  
756 the coupling of the system even before genesis (Figs.14d,e and 15d,e). When  
757 the trough moves towards the low-level warm advection, the genesis occurs,  
758 probably due to the consequent reduction of vertical stability. This sequence  
759 of events in the SE-BR winter genesis is defined as type B development by  
760 Petterssen and Smebye (1971).

761 It is important to note that, in the summer, the weak upper-level jet  
762 (Fig.9a) along with strong moisture convergence at low levels and the diffluent  
763 flow at upper levels are typical of subtropical cyclone development (Gozzo  
764 et al, 2014; Dutra et al, 2017). Subtropical cyclones in the South Atlantic de-  
765 velop mainly in the SE-BR region (Gozzo et al, 2014), and they may have been  
766 included in the composite process since no distinction between subtropical and  
767 extratropical cyclones is made.

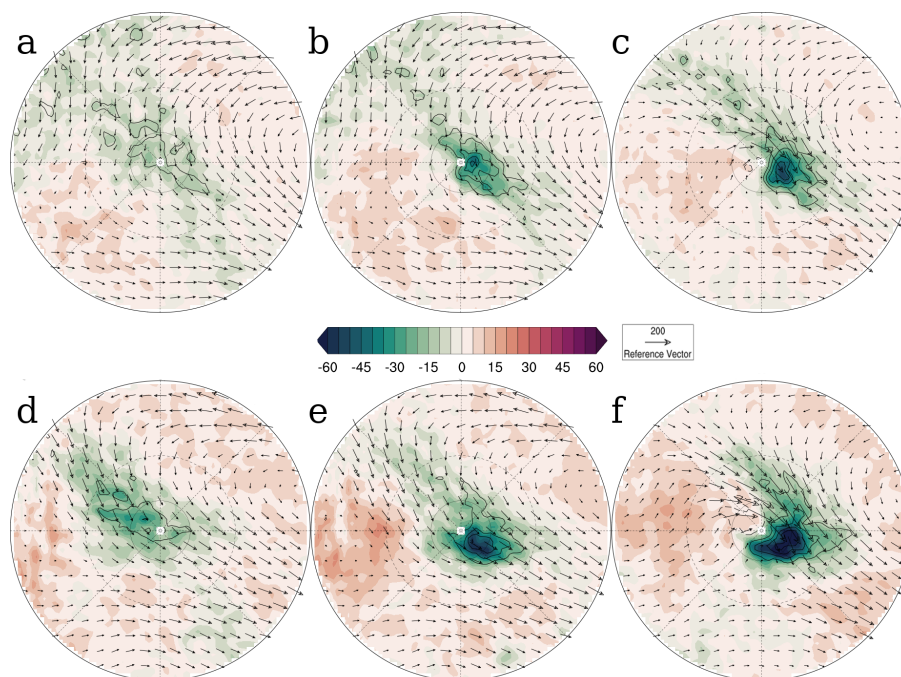


**Fig. 14** Composites of SE-BR cyclones omega at 700 hPa ( $10^{-2} Pa s^{-1}$ ; shaded), vertically integrated moisture transport ( $kg m^{-1} s^{-1}$ ; arrows) and moisture flux convergence ( $10^{-3} kg m^{-2} s^{-1}$ ; contour) at low level (1000 - 700 hPa) in the (a-c) summer and (d-f) winter: (a,d) at 12 hours before time of genesis; (b,e) at time of genesis, and; (c,f) at 24 hours after genesis. The vertical velocity is contoured every  $0.2 \times 10^{-3} kg m^{-2} s^{-1}$ , without the zero line and negative values (downward movement) are in dashed line.

### 768 5.2.2 La Plata region (LA PLATA)

769 The composites of mean thermal advection and winds at 850 hPa and geopo-  
 770 tential height at 500 hPa before and after genesis for cyclones from the LA  
 771 PLATA region are shown in Figs.16a-c, for the winter. Only the winter com-  
 772 posites are shown as this season has more cyclogenesis than summer but the  
 773 composites produced are similar for both seasons. The differences between the  
 774 summer and winter composites will be discussed in the text. The signature of  
 775 the Andes Cordillera, particularly in the composites before genesis time and  
 776 at genesis is apparent. This signal appears as a thin meridional strip of cold  
 777 advection. Warm advection exists at the center of cyclone before genesis time  
 778 in the winter composites, while it starts only at the time of genesis in the  
 779 summer composites. This warm advection in the winter composite seems to  
 780 be intensified by the anticyclonic circulation northeast of the cyclone center,  
 781 which may be the effect of the SASH westward shift in this season. In both  
 782 seasons the intensification of the warm and cold advection around the cyclone  
 783 center is faster after genesis time. Although the LA PLATA cyclones start

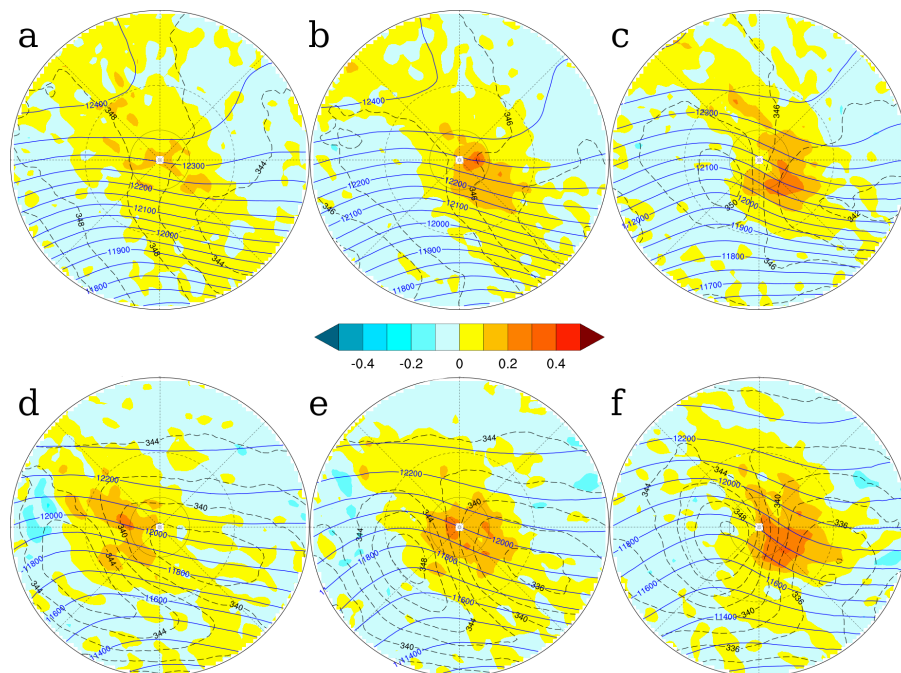


**Fig. 15** Composites of SE-BR cyclones potential temperature ( $K$ ; dashed line), geopotential height (gpm; blue line) and divergence of mass ( $s^{-1}$ ; shaded) at 200 hPa in the (a-c) summer and (d-f) winter: (a,d) at 12 hours before time of genesis; (b,e) at time of genesis, and; (c,f) at 24 hours after genesis.

784 over the continent, they move eastward over the ocean very quickly due to the  
 785 narrow shape of South America. In this way, they may be already over the  
 786 ocean at 12 to 24 hours after the genesis time, where surface fluxes can be  
 787 intense. In fact, the more intense temperature advection in the winter after  
 788 genesis can be understood in terms of the northward shift of the BMC. Figures  
 789 16d-f show the vertical velocity at 700 hPa, and the integrated moisture flux  
 790 convergence and transport. In the winter, it is possible to see subsidence in a  
 791 meridional strip promoted by descending air from the Andes Cordillera.

792 The elongated shape of the low observed in composites at the genesis  
 793 time (Figs.11b and f) makes us believe that it is an influence of the thermal-  
 794 orographic lows called Northwestern Argentina Low (NAL, Seluchi et al, 2003)  
 795 and the Chaco Low (CL, Saulo et al, 2004). The NAL is thermally induced in  
 796 summer due to surface fluxes above a desert region and orographically induced  
 797 in winter by forced subsidence during an upper-level trough occurrence and  
 798 is usually located around  $30^{\circ}S$  close to the Andes lee slope. The CL is basi-  
 799 cally thermally induced and is located further to the north around  $20^{\circ}S$  above  
 800 Paraguay and Bolivia (Seluchi and Saulo, 2012). The southward low level cir-  
 801 culation combined by CL and NAL allows a well-organized low-level northerly  
 802 current. The presence of the SASH westward of its main position linked with

803 the CL and NAL southward circulation in the winter may be responsible for  
804 the intensified warm advection before genesis. In the summer, the CL intensi-  
805 fies the transport of humidity to the LA PLATA region (Saulo et al, 2004), that  
806 may help the genesis. The tracking algorithm used here identifies the earlier  
807 stages of the cyclones that intensify further eastward, near the Southeastern  
808 South American coast and where using MSLP would first identify them. This  
809 fact reinforces the argument for the influence of thermal-orographic lows in the  
810 cyclogenesis in the LA PLATA region in both seasons, enhancing the moisture  
811 transport and warm advection. Ribeiro et al (2016) show that development  
812 of warm fronts in this region are related to the eastern edge of the CL and  
813 NAL northwesterly flow and, most of the time, are followed by cyclogenesis.  
814 Also, Seluchi et al (2003) and Seluchi and Saulo (1998) highlight the role of  
815 NAL formation in the reduction of static stability before genesis time due to  
816 warm and moist advection. The upper-level pattern of the LA PLATA cyclone  
817 composites (Figs.16g-i) is similar to the SE-BR cyclones. In the summer, the  
818 presence of a diffluent flow promotes divergence that enhances and organizes  
819 the low-level convergence at the genesis time (not shown), similar to the SE-  
820 BR composites. In the winter LA PLATA composites, there is an upper-level  
821 trough moving eastward reinforcing the low-level system.

### 822 5.2.3 Argentina region (ARG)

823 Although composites for the ARG cyclones were produced for summer and  
824 winter, only summer composites are presented here. Very few aspects are dif-  
825 ferent between the summer and winter composites and are discussed in the  
826 text. Figures 17a-c show the composite of the mean temperature advection  
827 and winds at 850 hPa and geopotential height at 500 hPa of the ARG cy-  
828 clones before, at and after genesis times for winter. In the ARG composites,  
829 as in the LA PLATA ones, the presence of the Andes Cordillera is observed  
830 through a meridional band of cold advection westward of the composite cen-  
831 ter. The mountain chain height at this latitude (45°S) is lower than at 30°S,  
832 and the lee effects are not so strong as in the LA PLATA region. However,  
833 it is possible to see a moving trough at 500 hPa that intensifies from -12h to  
834 genesis time due to low-level cold air advection and/or its interaction with  
835 the Andes stationary trough (e.g., Gan and Rao, 1994). In the ARG cyclone  
836 composites, the cold advection is stronger at the time of genesis, particularly  
837 in the summer. This strong cold advection occurs above the land surface, that  
838 is warmer than the upper air temperature in the summer, decreasing the static  
839 stability at the low level. In the winter, the reduction of static stability is lower  
840 as the cold advection is less intense. When compared with the SE-BR and LA  
841 PLATA cyclones, the ARG cyclone temperature advection intensifies rapidly  
842 in the 12 h interval after genesis time (not shown). Figures 17d-f present the  
843 vertical velocity at 700 hPa, and the integrated moisture flux convergence and  
844 transport and Figs.17g-i show the upper level geopotential (200 hPa) and the  
845 divergence of winds at 200 hPa. It is possible to see the 500 hPa geopotential  
846 trough westward of the composite cyclone center inducing upward vertical mo-

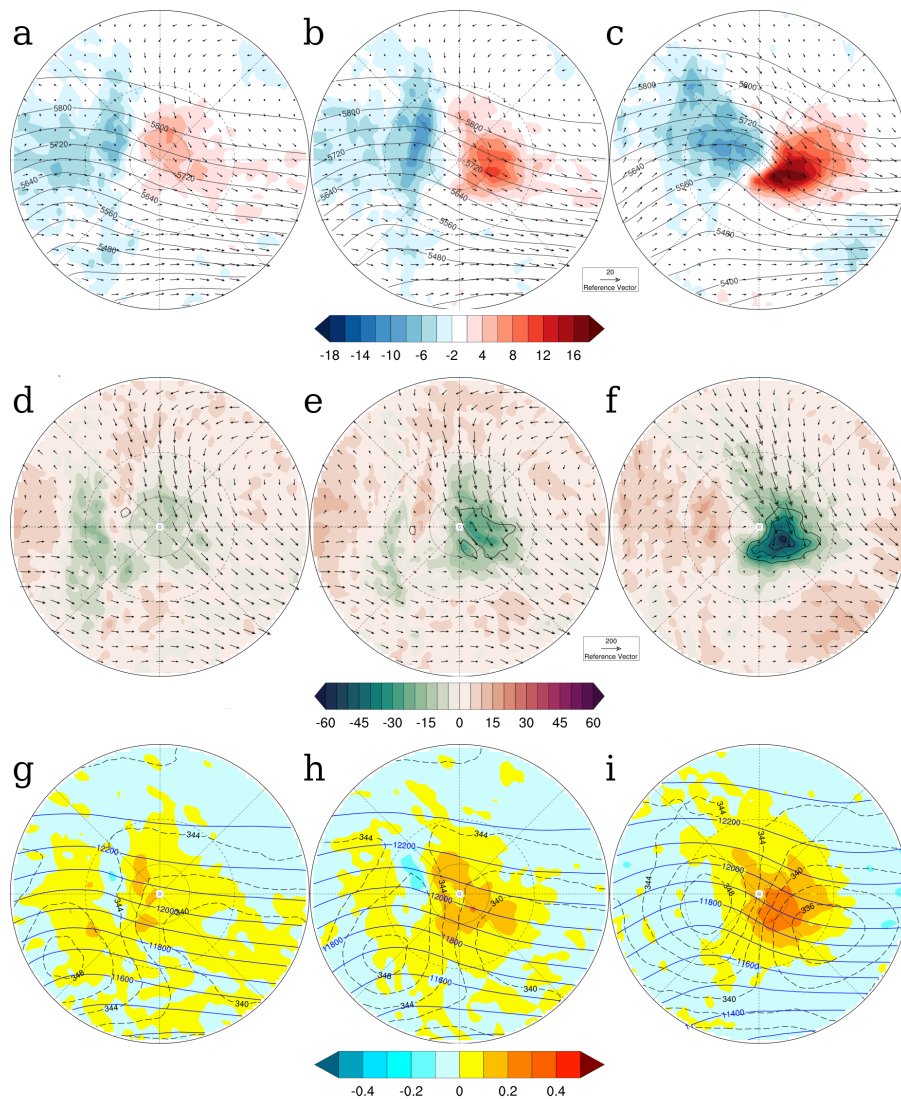


**Fig. 16** Composites of LA PLATA cyclones in the winter: (a-c) temperature advection at 850 hPa ( $10^{-5} K s^{-1}$ ; shaded), geopotential height at 500 hPa (gpm; blue line) and winds at 850 hPa ( $ms^{-1}$ ); (d-f) omega at 700 hPa ( $10^{-2} Pa s^{-1}$ ; shaded), vertically integrated moisture transport ( $kg m^{-1} s^{-1}$ ; arrows) and moisture flux convergence ( $10^{-3} kg m^{-2} s^{-1}$ ; contour) at low level (1000 - 700 hPa), and; (g-i) potential temperature ( $K$ ; dashed line), geopotential height (gpm; blue line) and divergence of mass ( $s^{-1}$ ; shaded) at 200 hPa. Composites (a,d,g) at 12 hours before the time of genesis; (b,e,h) at the time of genesis, and; (c,f,i) at 24 hours after the time of genesis. The vertical velocity is contoured every  $0.2 \times 10^{-3} kg m^{-2} s^{-1}$ , without the zero line and negative values (downward movement) are in dashed line.

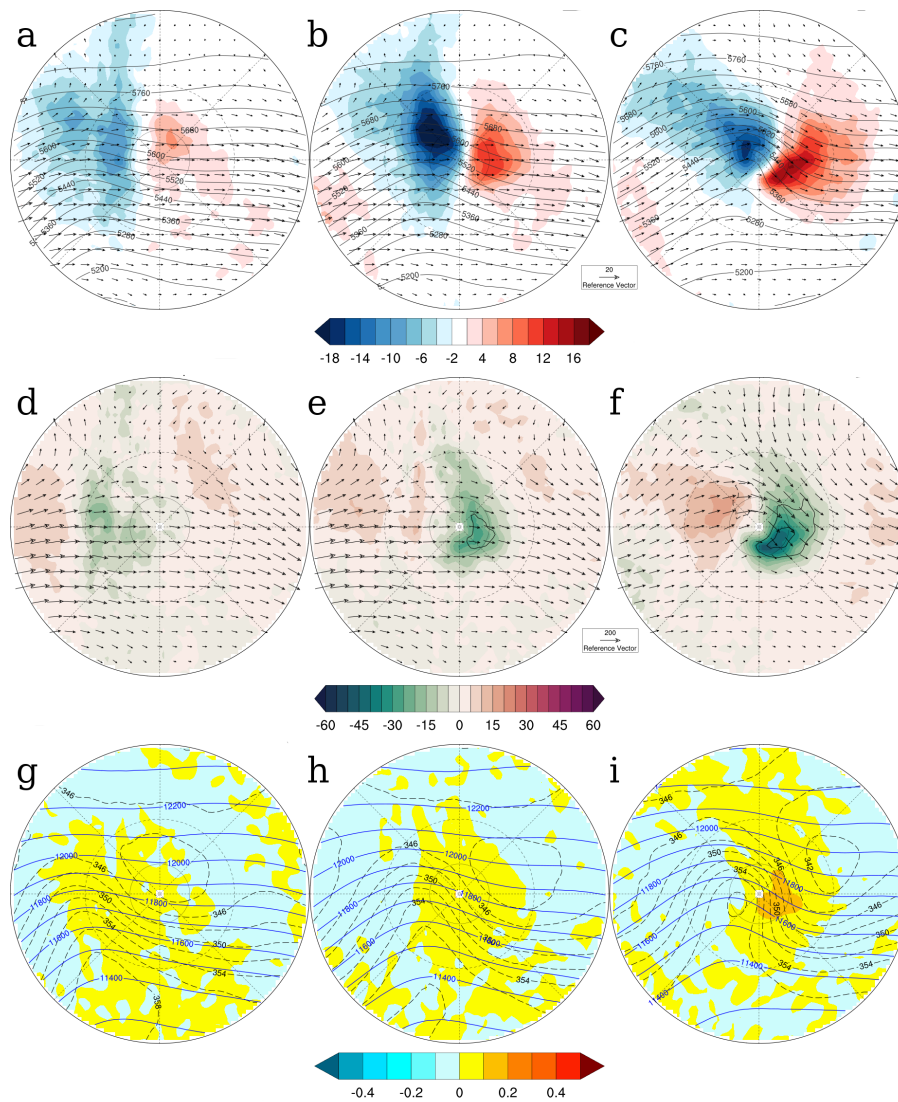


**Fig. 17** As in Fig.16 but for the composites of ARG cyclones in the summer.

847 tion. This baroclinic system is reinforced by an upper-level trough (Fig.17h).  
 848 There is no strong influence of horizontal moisture transport and low-level  
 849 convergence in the ARG region genesis process.

#### 850 5.2.4 Southeastern South Atlantic Ocean (SE-SAO)

851 Only cyclone composites from winter are shown here for the SE-SAO region,  
 852 for clarity. Again, differences between summer and winter composites will be

853 highlighted in the text. The winter composites of the mean temperature advec-  
854 tion and winds at 850 hPa and geopotential height at 500 hPa before and after  
855 genesis for SE-SAO cyclones are presented in Figs.18a-c. This shows there is a  
856 strong warm advection 12 hours before genesis in the center of the composite  
857 together with a cold advection westward. This cold advection at lower levels  
858 seems to be associated with the mid-level trough at 12h before genesis. The  
859 cold and warm advection increases rapidly after genesis time, being slightly  
860 stronger in the winter. The vertical velocity, vertically integrated moisture  
861 transport and moisture flux convergence are shown in Figs.18d-f. There is a  
862 convergence of moisture near the cyclone center 12h before the genesis time  
863 associated with a strong upward movement at 700 hPa. At the time of gen-  
864 esis, the 500 hPa trough moves eastward into the low-level warm advection  
865 region and reinforces the upward motion of moist and warm air. The SE-SAO  
866 cyclones seem to develop northwestward of another cyclone as it is possible  
867 to see through the curvature of the geopotential field at 500 hPa (Fig.18b)  
868 and MSLP structure at the time of genesis (Figs.11d and h). This secondary  
869 development occurs on the cold side of the parent cyclone. Some authors have  
870 related secondary development in the cold sector associated with the intrusion  
871 of dry stratospheric air (e.g., Browning et al, 1997; Iwabe and da Rocha, 2009).  
872 In fact, at the time of genesis, SE-SAO cyclones present a dry slot associated  
873 with intense cyclonic PV at 300 hPa in the cold sector close to their center  
874 (Figs.12d and h). The evidence of secondary cyclogenesis is in agreement with  
875 the high initial vorticity of the SE-SAO cyclones (Fig. 4 and Table 3). The  
876 major part of case studies (not shown) showed SE-SAO cyclones developing  
877 within the cold front and cold sector of a parental cyclone located south-  
878 eastward. There were also minority cases of downward development, with the  
879 parental cyclone placed west/northwestward.

## 880 6 Summary and Final Remarks

881 The paper has produced a new climatology for the entire South Atlantic do-  
882 main, including the open ocean, to provide new insights into the conditions  
883 leading to genesis in different regions of the South Atlantic. Two scientific  
884 questions were addressed (i) What are the main forcing mechanisms that con-  
885 trol cyclone development in each genesis region of the South Atlantic in their  
886 most active season?; and, (ii) Are there any differences in the genesis pre-  
887 cursors and structure of intense cyclones that originate in distinct genesis  
888 regions? The climatologies obtained by this study are in general in agreement  
889 with previous studies that found a main South Atlantic storm track between  
890 40°S and 55°S and a subtropical path coming from Uruguay (35°S) and the  
891 Southern Brazilian coast (30°S). The genesis density statistic indicates three  
892 main cyclogenesis regions on the South American coast: the Southern Brazilian  
893 coast (SE-BR, 30°S), above the continent near the La Plata river discharge  
894 region (LA PLATA, 35°S) and the southeastern coast of Argentina (ARG,  
895 40°S-55°S). A fourth genesis region was found centered at 45°S and 10°W

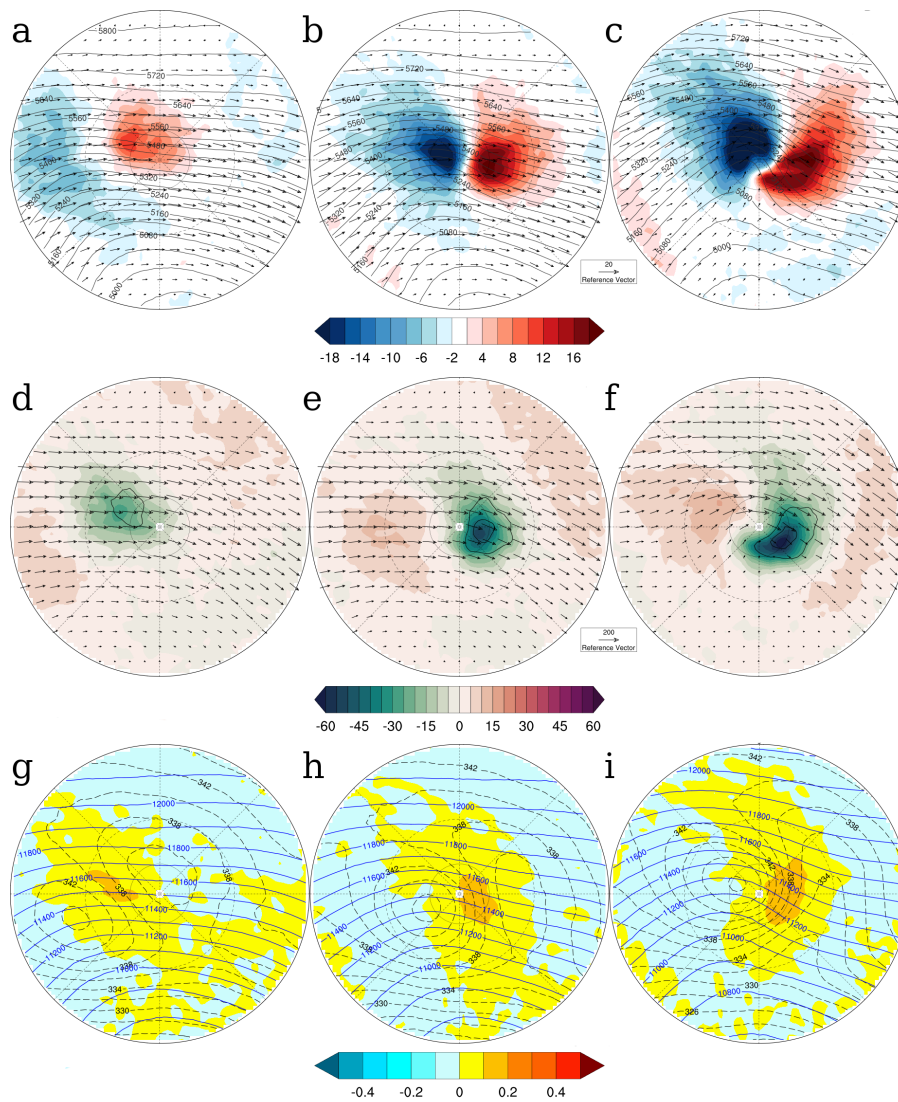


**Fig. 18** As in Fig.16 but for the composites of SE-SAO cyclones in the winter.

896 in the Southeastern South Atlantic (SE-SAO). The adjustment of the track-  
 897 ing constraints done to avoid tracking issues over South America improved  
 898 the identification of genesis, particularly in the ARG and SE-BR. The genesis  
 899 density maps show that the SE-BR and ARG regions are more active in the  
 900 summer (DJF) while the LA PLATA and SE-SAO regions are more active  
 901 in the winter, as reported by Hoskins and Hodges (2005) and Reboita et al  
 902 (2010a). However, the seasonal variability is not evident for the SE-BR and  
 903 ARG regions according to the numbers of cyclones per region.

904 We produced spatial distribution maps of the cyclone characteristics, in-  
905 cluding information from their genesis environment to answer the first scien-  
906 tific question. We found differences in the genesis environment of the South  
907 Atlantic domain. Northward of 35°S, two distinct processes lead to genesis in  
908 the summer and winter. In the summer, low-level forcing is more critical in  
909 the genesis process, primarily associated with moisture transport. In the win-  
910 ter, a stronger upper-level jet may play an important role in genesis through  
911 baroclinic instability. Moreover, the northward shift of the SST gradient near  
912 the Southeastern South American coast may be an essential feature of gene-  
913 sis and intensification at 35°S. Southward of 35°S, cyclones develop in a high  
914 baroclinic environment with a smaller influence of low-level humidity when  
915 compared to the other regions.

916 The second science question concerns the differences in the genesis precu-  
917 sors of cyclones generated in different genesis regions of the domain. To answer  
918 this we performed radial composites of mean fields before, at the time of genesis  
919 and after. We found similarities and differences between the genesis precursors  
920 for each region. The intense cyclones of all regions are influenced by a mid-  
921 level trough giving dynamical support to the genesis. Although, cyclones from  
922 the SE-BR and LA PLATA present a stronger low-level forcing when compar-  
923 ed to the ARG and SE-SAO cyclones. Cyclone composites reinforce the im-  
924 portance of moisture fluxes to genesis in the SE-BR region, including evi-  
925 dence of secondary development on trailing fronts during the summer. The LA  
926 PLATA cyclone development is supported by the warm advection promoted  
927 by the thermal-orographic lows (CL and NAL) on the lee side of the Andes.  
928 The ARG cyclone genesis is mainly associated with traditional baroclinic de-  
929 velopment, reinforced by the interaction of mid-level troughs with the Andes  
930 and the low static stability in the summer. The SE-SAO cyclones develop in  
931 a high baroclinic region in the cold sector of a parent cyclone.

932 There are extensive efforts to study and understand climate change, and  
933 this work contributes to the formulation of the questions and hypothesis to  
934 what we can expect about changes in cyclone behavior in the South Atlantic.  
935 Several studies have shown a decrease in cyclone activity over the globe jus-  
936 tified by the reduction of low-level baroclinicity (e.g., Geng and Sugi, 2003).  
937 However, the effect of the moistening in a warmer climate to cyclones is still  
938 not clear (e.g., Schneider et al, 2010). Thus, our findings indicate that differ-  
939 ent South Atlantic genesis regions may respond differently to climate change  
940 where they have distinct forcing mechanisms. This will be investigated fur-  
941 ther in future work using climate models, e.g., CMIP5/CMIP6 models, and  
942 dynamical downscaling.

943 **Acknowledgements** The authors acknowledge financial support provided by the Conselho  
944 Nacional de Desenvolvimento Científico e Tecnológico - Brasil (CNPq) - Grant 141658/2015-  
945 0 - and the Coordenação de Aperfeiçoamento de Pessoal de Nível Superior - Brasil (CAPES)  
946 - Finance Code 001. The CFSR data was developed by NOAA's National Centers for Envi-  
947 ronmental Prediction (NCEP). The data for this study are from NOAA's National Oper-  
948 ational Model Archive and Distribution System (NOMADS), which is maintained at NOAA's  
949 National Centers for Environmental Information (NCEI).

**References**

- 950 **References**
- 951 Bengtsson L, Hodges KI, Easch M, Keenlyside N, Kornbluh L, Luo JJ, Ya-  
952 magata T (2007) How may tropical cyclones change in a warmer climate?  
953 *Tellus* 59A:539–561, DOI 10.1111/j.1600-0870.2007.00251.x
- 954 Bengtsson L, Hodges KI, Keenlyside N (2009) Will extratropical storms  
955 intensify in a warmer climate? *J Climate* 22(9):2276–2301, DOI  
956 10.1175/2008JCLI2678.1
- 957 Berbery EH, Vera CS (1996) Characteristics of the Southern Hemisphere win-  
958 ter storm track with filtered and unfiltered data. *J Atmos Sci* 53(3):468–481
- 959 Bjerknes J, Solberg H (1922) Life cycle of cyclones and the polar front theory  
960 of atmospheric circulation. *Geophys Publ* 3:1–18
- 961 Bluestein H (1992) *Synoptic-Dynamic Meteorology in Midlatitudes: Principles*  
962 *of Kinematics and Dynamics*, Vol. 1. Oxford University Press
- 963 Bolton D (1980) The computation of equivalent potential temperature. *Mon*  
964 *Wea Rev* 108:1046–1053
- 965 Browning KA, Roberts NM (1994) Structure of a frontal cyclone. *Quart J Roy*  
966 *Meteor Soc* 120(520):1535–1557, DOI 10.1002/qj.49712052006
- 967 Browning KA, Roberts NM, Illingworth AJ (1997) Mesoscale analysis of the  
968 activation of a cold front during cyclogenesis. *Quart J Roy Meteor Soc*  
969 123(544):2349–2374, DOI 10.1002/qj.49712354410
- 970 Campos EJD, Lentini CAD, Miller JL, Piola AR (1999) Interannual variability  
971 of the sea surface temperature in the South Brazil Bight. *Geophys Res Lett*  
972 26(14):2061–2064, DOI 10.1029/1999GL900297
- 973 Catto JL, Shaffrey LC, Hodges KI (2010) Can climate models capture  
974 the structure of extratropical cyclones? *J Climate* 23(7):1621–1635, DOI  
975 10.1175/2009JCLI3318.1
- 976 da Rocha RP, Sugahara S, da Silveira RB (2004) Sea waves generated by  
977 extratropical cyclones in the South Atlantic Ocean: Hindcast and validation  
978 against altimeter data. *Wea Forecasting* 19(2):398–410, DOI 10.1175/1520-  
979 0434(2004)019;0398:SWGEBEC;2.0.CO;2
- 980 Dacre HF, Gray SL (2006) Life-cycle simulations of shallow frontal waves and  
981 the impact of deformation strain. *Quart J Roy Meteor Soc* 132(620):2171–  
982 2190, DOI 10.1256/qj.05.238
- 983 Dacre HF, Gray SL (2009) The Spatial Distribution and Evolution Charac-  
984 teristics of North Atlantic Cyclones. *Mon Wea Rev* 137:99–115
- 985 Dacre HF, Hawcroft MK, Stringer MA, Hodges KI (2012) An Extratropical  
986 Cyclone Atlas: A tool for illustrating cyclone structure and evolution char-  
987 acteristics. *Bull Amer Meteor Soc* 93(10):1497–1502, DOI 10.1175/BAMS-  
988 D-11-00164.1
- 989 Dias Pinto JR, Da Rocha RP (2011) The energy cycle and structural evolution  
990 of cyclones over southeastern South America in three case studies. *J Geophys*  
991 *Res: Atmos* 116(14):1–17, DOI 10.1029/2011JD016217
- 992 Dias Pinto JR, Reboita MS, Da Rocha RP (2013) Synoptic and dynamical  
993 analysis of subtropical cyclone Anita (2010) and its potential for tropi-  
994 cal transition over the South Atlantic Ocean. *J Geophys Res: Atmos*

- 118(19):10,870–10,883, DOI 10.1002/jgrd.50830
- 995 Drumond A, Nieto R, Gimeno L, Ambrizzi T (2008) A Lagrangian identifica-  
996 tion of major sources of moisture over Central Brazil and La Plata Basin. *J*  
997 *Geophys Res: Atmos* 113(D14), DOI 10.1029/2007JD009547
- 998 Dutra LMM, da Rocha RP, Lee RW, Peres JRR, de Camargo R (2017)  
999 Structure and evolution of subtropical cyclone Anita as evaluated by heat  
1000 and vorticity budgets. *Quart J Roy Meteor Soc* 143(704):1539–1553, DOI  
1001 10.1002/qj.3024
- 1002 Ek MB, Mitchell KE, Lin Y, Rogers E, Grunmann P, Koren V, Gayno  
1003 G, Tarpley JD (2003) Implementation of noah land surface model ad-  
1004 vances in the national centers for environmental prediction operational  
1005 mesoscale eta model. *J Geophys Res: Atmos* 108(D22):n/a–n/a, DOI  
1006 10.1029/2002JD003296, 8851
- 1007 Funatsu BM, Gan MA, Caetano E (2004) A case study of orographic cycloge-  
1008 nesis over South America. *Atmosfera* 17(2):91–113
- 1009 Gan MA, Rao VB (1991) Surface Cyclogenesis over South America. *Mon Wea*  
1010 *Rev* 119:1293–1302
- 1011 Gan MA, Rao VB (1994) The influence of the Andes Cordillera on tran-  
1012 sient disturbances. *Mon Wea Rev* 122:1141–1157, DOI 10.1175/1520-  
1013 0493(1994)122;1141:TOTAC;2.0.CO;2
- 1014 Geng Q, Sugi M (2003) Possible change of extratropical cyclone activity  
1015 due to enhanced greenhouse gases and sulfate aerosols - Study with a  
1016 high-resolution AGCM. *J Climate* 16(13):2262–2274, DOI 10.1175/1520-  
1017 0442(2003)16;2262:PCOECA;2.0.CO;2
- 1018 Gordon AL (1989) Brazil-Malvinas Confluence - 1984. *Deep Sea Re-*  
1019 *search Part A Oceanographic Research Papers* 36(3):359 – 384, DOI  
1020 [https://doi.org/10.1016/0198-0149\(89\)90042-3](https://doi.org/10.1016/0198-0149(89)90042-3)
- 1021 Gozzo LF, da Rocha RP (2013) Air-sea interaction processes influencing  
1022 the development of a Shapiro-Keyser type cyclone over the Subtropical  
1023 South Atlantic Ocean. *Pure and Applied Geophysics* 170(5):917–934, DOI  
1024 10.1007/s00024-012-0584-3
- 1025 Gozzo LF, da Rocha RP, Reboita MS, Sugahara S (2014) Subtropical cyclones  
1026 over the southwestern South Atlantic: Climatological aspects and case study.  
1027 *J Climate* 27(22):8543–8562, DOI 10.1175/JCLI-D-14-00149.1
- 1028 Griffies S, Harrison MJ, Pacanowski RC, Rosati A (2004) A technical guide  
1029 to MOM4. GFDL Ocean Group Tech. Rep. 5, NOAA/Geophysical Fluid  
1030 Dynamics Laboratory, version prepared on August 23, 2004
- 1031 Grise KM, Son SW, Gyakum JR (2013) Intraseasonal and interannual vari-  
1032 ability in North American storm tracks and its relationship to Equatorial  
1033 Pacific variability. *Mon Wea Rev* 141(10):3610–3625, DOI 10.1175/MWR-  
1034 D-12-00322.1
- 1035 Hodges KI (1994) A general-method for tracking analysis and its application to  
1036 meteorological data. *Mon Wea Rev* 122(11):2573–2586, DOI 10.1175/1520-  
1037 0493(1994)122;2573:AGMFTA;2.0.CO;2
- 1038 Hodges KI (1995) Feature tracking on the unit sphere.  
1039 *Mon Wea Rev* 123(12):3458–3465, DOI 10.1175/1520-  
1040

- 1041 0493(1995)123;3458:FTOTUS;2.0.CO;2
- 1042 Hodges KI (1996) Spherical nonparametric estimators applied to the UGAMP  
1043 model integration for AMIP. *Mon Wea Rev* 124(12):2914–2932, DOI  
1044 10.1175/1520-0493(1996)124;2914:SNEATT;2.0.CO;2
- 1045 Hodges KI (1999) Adaptive Constraints for Feature Tracking. *Mon Wea Rev*  
1046 127:1362–1373, DOI 10.1175/1520-0493(1999)127;1362:ACFFT;2.0.CO;2
- 1047 Hodges KI, Lee RW, Bengtsson L (2011) A Comparison of Extratropical Cy-  
1048 clones in Recent Reanalyses ERA-Interim, NASA MERRA, NCEP CFSR,  
1049 and JRA-25. *J Climate* 24:4888–4906, DOI 10.1175/2011JCLI4097.1
- 1050 Hoskins A, Hodges KI (2005) A New Perspective on the Southern Hemisphere  
1051 Storm Tracks. *J Climate* 18:4108–4129
- 1052 Hoskins BJ, Hodges KI (2002) New Perspectives on the Northern Hemi-  
1053 sphere Winter Storm Tracks. *J Atmos Sci* 59:1041–1061, DOI 10.1175/1520-  
1054 0469(2002)059;1041:NPOTNH;2.0.CO;2
- 1055 Inatsu M, Hoskins BJ (2004) The zonal asymmetry of the Southern Hemi-  
1056 sphere winter storm track. *J Climate* 17(24):4882–4892, DOI 10.1175/JCLI-  
1057 3232.1
- 1058 Innocentini V, Neto EDSC (1996) A case study of the 9 august 1988 South  
1059 Atlantic storm: Numerical simulations of the wave activity. *Wea Forecasting*  
1060 11(1):78–88, DOI 10.1175/1520-0434(1996)011;0078:ACSOTA;2.0.CO;2
- 1061 Iwabe CMN, da Rocha RP (2009) An event of stratospheric air intrusion and  
1062 its associated secondary surface cyclogenesis over the south atlantic ocean.  
1063 *J Geophys Res: Atmospheres* 114(D9), DOI 10.1029/2008JD011119, d09101
- 1064 Iwabe CMN, Reboita MS, de Camargo R (2011) Estudo de caso de uma  
1065 situação atmosférica entre 12 e 19 de setembro de 2008 com algumas car-  
1066 acterísticas semelhantes ao evento catarina. *Rev Bras Meteorol* 26(March  
1067 2011):67–84
- 1068 Jones DA, Simmonds I (1993) A climatology of Southern Hemisphere extrat-  
1069 ropical cyclones. *Climate Dyn* 9(3):131145, DOI 10.1007/BF00209750
- 1070 Kanamitsu M, Ebisuzaki W, Woollen J, Yang SK, Hnilo JJ, Fiorino M, Potter  
1071 GL (2002) NCEP/DOE AMIP-II Reanalysis (R-2). *Bull Amer Meteor Soc*  
1072 83(11):1631–1644, DOI 10.1175/BAMS-83-11-1631
- 1073 Krüger LF, da Rocha RP, Reboita MS, Ambrizzi T (2012) RegCM3 nested in  
1074 HadAM3 scenarios A2 and B2: Projected changes in extratropical cyclogene-  
1075 sis, temperature and precipitation over the South Atlantic Ocean. *Climatic*  
1076 *Change* 113(3-4):599–621, DOI 10.1007/s10584-011-0374-4
- 1077 Marengo JA, Soares WR, Saulo C, Nicolini M (2004) Climatology of the low-  
1078 level jet east of the Andes as derived from the NCEP–NCAR Reanalyses:  
1079 Characteristics and temporal variability. *J Climate* 17(12):2261–2280, DOI  
1080 10.1175/1520-0442(2004)017;2261:COTLJE;2.0.CO;2
- 1081 Mendes D, Souza EP, Trigo F Isabel, Miranda PMA (2007) On precursors  
1082 of South American cyclogenesis. *Tellus* 59A:114–121, DOI 10.1111/j.1600-  
1083 0870.2006.00215.x
- 1084 Mendes D, Souza EP, Marengo J, Mendes MCD (2010) Climatology of extra-  
1085 tropical cyclones over the South American-southern oceans sector. *Theo-*  
1086 *retical and Applied Climatology* 100(3):239–250, DOI 10.1007/s00704-009-

0161-6

- 1087  
1088 Murray FW (1967) On the computation of saturation vapor  
1089 pressure. *J Appl Meteor* 6(1):203–204, DOI 10.1175/1520-  
1090 0450(1967)006;0203:OTCOSV;2.0.CO;2
- 1091 Murray RJ, Simmonds I (1991) A numerical scheme for tracking cyclone centres  
1092 from digital data Part II: application to January and July general circulation  
1093 model simulations. *Australian Meteorological Magazine* 39:167–180
- 1094 Olson DB, Podest GP, Evans RH, Brown OB (1988) Temporal variations in the  
1095 separation of Brazil and Malvinas currents. *Deep Sea Research Part A Oceanographic  
1096 Research Papers* 35(12):1971 – 1990, DOI  
1097 [https://doi.org/10.1016/0198-0149\(88\)90120-3](https://doi.org/10.1016/0198-0149(88)90120-3)
- 1098 Orlandi I, Katzfey J (1991) The life cycle of a cyclone wave in the Southern  
1099 Hemisphere. Part I: Eddy energy budget. *J Atmos Sci* 48(17):1972–1998,  
1100 DOI 10.1175/1520-0469(1991)048;1972:TLCOAC;2.0.CO;2
- 1101 Parise CK, Calliari LJ, Krusche N (2009) Extreme storm surges in the south  
1102 of Brazil: atmospheric conditions and shore erosion. *Braz J Oceanogr* 57:175  
1103 – 188, DOI 10.1590/S1679-87592009000300002
- 1104 Petterssen S, Smebye SJ (1971) On the development of extratropical cyclones.  
1105 *Quart J Roy Meteor Soc* 97(414):457–482, DOI 10.1002/qj.49709741407
- 1106 Piola AR, Campos EJD, Möller OO, Charo M, Martinez C (2000) Subtropical  
1107 shelf front off eastern south america. *J Geophys Res: Oceans* 105(C3):6565–  
1108 6578, DOI 10.1029/1999JC000300
- 1109 Piva ED, Moscati MCdL, Gan MA (2008) Papel dos fluxos de calor latente e  
1110 sensível em superfície associado a um caso de ciclogênese na costa leste da  
1111 América do Sul. *Rev Bras Meteorol* 23(4):450–476
- 1112 Piva ED, Gan MA, Rao VB (2010) Energetics of winter troughs entering South  
1113 America. *Mon Wea Rev* 138(4):1084–1103, DOI 10.1175/2009MWR2970.1
- 1114 Piva ED, Gan MA, Moscati MCdL (2011) The role of latent and sensible heat  
1115 fluxes in an explosive cyclogenesis over the South American East Coast. *J  
1116 Meteor Soc Japan* 89(6):637–663, DOI 10.2151/jmsj.2011-604
- 1117 Reboita MS, Ambrizzi T, da Rocha RP (2009) Relationship between the southern  
1118 annular mode and southern hemisphere atmospheric systems. *Rev Bras  
1119 Meteorol* 24:48–55, DOI 10.1590/S0102-77862009000100005
- 1120 Reboita MS, da Rocha RP, Ambrizzi T, Sugahara S (2010a) South Atlantic  
1121 Ocean cyclogenesis climatology simulated by regional climate model  
1122 (RegCM3). *Climate Dyn* 35(7-8):1331–1347, DOI 10.1007/s00382-009-0668-  
1123 7
- 1124 Reboita MS, Gan MA, da Rocha RP, Ambrizzi T (2010b) Precipitation regimes  
1125 in South America: a bibliography review. *Rev Bras Meteorol* 25:185 – 204,  
1126 DOI 10.1590/S0102-77862010000200004
- 1127 Reboita MS, da Rocha RP, de Souza MR, Llopart M (2018) Extratropical  
1128 cyclones over the southwestern South Atlantic Ocean: HadGEM2–ES and  
1129 RegCM4 projections. *Int J Climatol* 0(0):1–14, DOI 10.1002/joc.5468
- 1130 Renfrew IA, Thorpe AJ, Bishop CH (1997) The role of the environmental flow  
1131 in the development of secondary frontal cyclones. *Quart J Roy Meteor Soc*  
1132 123(542):1653–1675, DOI 10.1002/qj.49712354210

- 1133 Ribeiro BZ, Seluchi ME, Chou SC (2016) Synoptic climatology of warm  
1134 fronts in Southeastern South America. *International Journal of Climatol-*  
1135 *ogy* 36(2):644–655, DOI 10.1002/joc.4373
- 1136 Saha S, Moorthi S, Pan HL, Wu X, Wang J, Nadiga S, Tripp P, Kistler R,  
1137 Woollen J, Behringer D, Liu H, Stokes D, Grumbine R, Gayno G, Wang J,  
1138 Hou YT, Chuang H, Juang HMH, Sela J, Iredell M, Treadon R, Kleist D,  
1139 Delst PV, Keyser D, Derber J, Ek M, Meng J, Wei H, Yang R, Lord S, Dool  
1140 H, Kumar A, Wang W, Long C, Chelliah M, Xue Y, Huang B, Schemm  
1141 JK, Ebisuzaki W, Lin R, Xie P, Chen M, Zhou S, Higgins W, Zou CZ, Liu  
1142 Q, Chen Y, Han Y, Cucurull L, Reynolds RW, Rutledge G, Goldberg M  
1143 (2010) The ncep climate forecast system reanalysis. *Bull Amer Meteor Soc*  
1144 91(8):1015–1058, DOI 10.1175/2010BAMS3001.1
- 1145 Sanders F, Gyakum JR (1980) Synoptic-dynamic climatology of  
1146 the bomb. *Mon Wea Rev* (10):1589–1606, DOI 10.1175/1520-  
1147 0493(1980)108;1589:SDCOT;2.0.CO;2
- 1148 Satyamurty P, Ferreira CC, Gan MA (1990) Cyclonic vortices over South  
1149 America. *Tellus A* 42(1):194–201
- 1150 Saulo AC, Seluchi ME, Nicolini M (2004) A case study of a Chaco Low-Level  
1151 Jet event. *Mon Wea Rev* 132(11):2669–2683, DOI 10.1175/MWR2815.1
- 1152 Schneider T, Gorman PAO, Levine XJ (2010) Water vapor and the dy-  
1153 namics of climate changes. *Reviews of Geophysics* 48(RG3001):1–22, DOI  
1154 10.1029/2009RG000302, URL <http://dx.doi.org/10.1029/2009RG000302>;
- 1155 Seluchi ME, Saulo AC (1998) Possible mechanisms yielding an explosive  
1156 coastal cyclogenesis over South America: experiments using a limited area  
1157 model. *Aust Meteor Mag* 47:309–320
- 1158 Seluchi ME, Saulo AC (2012) Baixa do Noroeste Argentino e Baixa do Chaco:  
1159 caracterisitcas, diferenças e semelhanças. *Rev Bras Meteorol* 27(1):49–60
- 1160 Seluchi ME, Saulo AC, Nicolini M, Satyamurty P (2003) The northwestern  
1161 argentinean low: A study of two typical events. *Mon Wea Rev* 131(10):2361–  
1162 2378, DOI 10.1175/1520-0493(2003)131;2361:TNALAS;2.0.CO;2
- 1163 Shapiro MA, Keyser D (1990) Fronts, jet streams and the tropopause. In:  
1164 Newton CW, Holopainen EO (eds) *Extratropical Cyclones, The Erik Palmen*  
1165 *Memorial Volume*, Amer. Meteor. Soc., pp 167–191
- 1166 Simmonds I, Keay K (2000) Mean southern hemisphere extratropical cyclone  
1167 behavior in the 40-year NCEP-NCAR reanalysis. *J Climate* 13(5):873–885,  
1168 DOI 10.1175/1520-0442(2000)013;0873:MSHECB;2.0.CO;2
- 1169 Sinclair MR (1994) An objective cyclone climatology for the South-  
1170 ern Hemisphere. *Mon Wea Rev* 122(10):2239–2256, DOI 10.1175/1520-  
1171 0493(1994)122;2239:AOCFFT;2.0.CO;2
- 1172 Sinclair MR (1995) A climatology of cyclogenesis for the Southern Hemisphere.  
1173 *Mon Wea Rev* 123:1601–1619
- 1174 Sinclair MR (1997) Objective identification of cyclones and their circulation in-  
1175 tensity, and climatology. *Wea Forecasting* 12(3):595–612, DOI 10.1175/1520-  
1176 0434(1997)012;0595:OIOCAT;2.0.CO;2
- 1177 Stopa JE, Cheung KF (2014) Intercomparison of wind and wave data from  
1178 the ECMWF Reanalysis Interim and the NCEP Climate Forecast System

- 1179 Reanalysis. *Ocean Modelling* 75:65–83, DOI 10.1016/j.ocemod.2013.12.006
- 1180 Streten NA, Troup AJ (1973) A synoptic climatology of satellite observed
- 1181 cloud vortices over the southern hemisphere. *Quart J Roy Meteor Soc*
- 1182 99(419):56–72, DOI 10.1002/qj.49709941906
- 1183 Sun X, Cook KH, Vizy EK (2017) The South Atlantic Subtropical
- 1184 High: Climatology and interannual variability. *J Climate* 30(9):3279–3296,
- 1185 DOI 10.1175/JCLI-D-16-0705.1, URL [https://doi.org/10.1175/JCLI-D-16-](https://doi.org/10.1175/JCLI-D-16-0705.1)
- 1186 [0705.1](https://doi.org/10.1175/JCLI-D-16-0705.1)
- 1187 Taljaard JJ (1967) Development, distribution and movement of cyclones and
- 1188 anticyclones in the Southern Hemisphere during the IGY. *J Appl Meteor*
- 1189 6(6):973–987, DOI 10.1175/1520-0450(1967)006<0973:DDAMOC>2.0.CO;2
- 1190 Trenberth KE (1991) Storm Tracks in the Southern Hemisphere. *J Atmos Sci*
- 1191 48(19):2159–2178
- 1192 Vera C, Higgins W, Amador J, Ambrizzi T, Garreaud R, Gochis D, Gutzler
- 1193 D, Lettenmaier D, Marengo J, Mechoso CR, Nogues-Paegle J, Dias PLS,
- 1194 Zhang C (2006) Toward a unified view of the American Monsoon Systems.
- 1195 *J Climate* 19(20):4977–5000, DOI 10.1175/JCLI3896.1
- 1196 Vera CS, Vighiarolo PK, Berbery EH (2002) Cold season synoptic-scale waves
- 1197 over subtropical South America. *Mon Wea Rev* 130(3):684–699, DOI
- 1198 [10.1175/1520-0493\(2002\)130<0684:CSSSWO>2.0.CO;2](https://doi.org/10.1175/1520-0493(2002)130<0684:CSSSWO>2.0.CO;2)